The Cerebellum (2021) 20:853–871
https://doi.org/10.1007/s12311-021-01249-4

ORIGINAL ARTICLE

# Feasibility of combining functional near-infrared spectroscopy with electroencephalography to identify chronic stroke responders to cerebellar transcranial direct current stimulation—a computational modeling and portable neuroimaging methodological study

Zeynab Rezaee[1] · Shashi Ranjan[2] · Dhaval Solanki[2] · Mahasweta Bhattacharya[1] · M. V. Padma Srivastava[3] · Uttama Lahiri[2] · Anirban Dutta[1]

Accepted: 21 February 2021 / Published online: 6 March 2021


## Abstract

Feasibility of portable neuroimaging of cerebellar transcranial direct current stimulation (ctDCS) effects on the cerebral cortex has not been investigated vis-à-vis cerebellar lobular electric field strength. We studied functional near-infrared spectroscopy (fNIRS) in conjunction with electroencephalography (EEG) to measure changes in the brain activation at the prefrontal cortex (PFC) and the sensorimotor cortex (SMC) following ctDCS as well as virtual reality–based balance training (VBaT) before and after ctDCS treatment in 12 hemiparetic chronic stroke survivors. We performed general linear modeling (GLM) that putatively associated the lobular electric field strength with the changes in the fNIRS-EEG measures at the ipsilesional and contra-lesional PFC and SMC. Here, fNIRS-EEG measures were found in the latent space from canonical correlation analysis (CCA) between the changes in total hemoglobin (tHb) concentrations (0.01–0.07Hz and 0.07–0.13Hz bands) and log10-transformed EEG bandpower within 1–45 Hz where significant (Wilks' lambda>0.95) canonical correlations were found only for the 0.07–0.13-Hz band. Also, the first principal component (97.5% variance accounted for) of the mean lobular electric field strength was a good predictor of the latent variables of oxy-hemoglobin (O2Hb) concentrations and log10-transformed EEG bandpower. GLM also provided insights into non-responders to ctDCS who also performed poorly in the VBaT due to ideomotor apraxia. Future studies should investigate fNIRS-EEG joint-imaging in a larger cohort to identify non-responders based on GLM fitting to the fNIRS-EEG data.

**Keywords** Transcranial direct current stimulation · Postural balance · Stroke · Cerebellum · fNIRS · EEG

Zeynab Rezaee and Shashi Ranjan are equal first authors.

Uttama Lahiri and Anirban Dutta are equal last authors.

✉ Anirban Dutta
anirband@buffalo.edu

Zeynab Rezaee
zeynabre@buffalo.edu

Shashi Ranjan
shashi.r@iitgn.ac.in

Dhaval Solanki
dhaval.solanki@iitgn.ac.in

Mahasweta Bhattacharya
mahaswet@buffalo.edu

M. V. Padma Srivastava
vasanthapadma123@gmail.com

Uttama Lahiri
uttamalahiri@iitgn.ac.in

[1] University at Buffalo, Buffalo, NY 14260, USA

[2] Indian Institute of Technology Gandhinagar, Ahmedabad, India

[3] All India Institute Of Medical Sciences, New Delhi, India

## Introduction

Non-invasive brain stimulation (NIBS) techniques are increasingly being applied to the cerebellum in clinical applications [1–3]; however, a rational approach to deliver and measure brain response to cerebellar NIBS is not available at the point of care settings. Such a rational approach is crucial for cerebellar NIBS methods, e.g., cerebellar transcranial direct current stimulation (ctDCS), due to large inter-subject and intra-subject variability in the effects [4]. Since transcranial direct current stimulation (tDCS) is increasingly being investigated as an adjunct treatment to facilitate home-based rehabilitation [5] due to its ease of use for various clinical applications [6], therefore, a rational approach to deliver and measure brain response to ctDCS needs immediate attention. We postulate that identifying responders to ctDCS due to post-stroke heterogenous brain lesions and ctDCS dosage considerations [7] for the responders in a home setting can be challenging without portable neuroimaging of the cerebral responses. We have highlighted using a portable neuroimaging method combining electroencephalography (EEG) and functional near-infrared spectroscopy (fNIRS) during anodal tDCS [8] that ischemic stroke can lead to dysfunction in neurovascular coupling [9]. Vascular-based functional brain imaging techniques, such as fMRI and fNIRS, rely on this neurovascular coupling to infer neural activity changes. The EEG can capture neural activity with excellent temporal (in milliseconds), but the low spatial resolution (in centimeters) [10]. The fNIRS, which is less susceptible to electrical noise, is a promising tool for monitoring cerebral metabolic changes with better spatial but lower temporal resolution due to the inherent hemodynamic delay [11]. In our previous study [8], an initial dip in the oxy-hemoglobin concentration during anodal tDCS-induced activation of the primary motor cortex (M1) region located under the electrodes and in-between the fNIRS light sources and detectors corresponded with an increase in the log-transformed mean-power of EEG within 0.5–11.25-Hz frequency band [8]. We also presented a computational pipeline to monitor cerebral tDCS-facilitated cortical reorganization [12]; however, the feasibility of such fNIRS-EEG joint-imaging of ctDCS effects on the cerebral cortex was not evaluated in our prior works. Since the cerebellum is related to movement function, especially gait and balance, and error-based motor learning, ctDCS has been proposed to facilitate motor adaptation during a balance learning task by Zandvliet and colleagues [13]. Moreover, the cerebellum's role in the cognitive aspect of motor learning is increasingly being recognized that is postulated based on ctDCS effects on the prefrontal cortex via closed-loop cerebro-cerebellar circuits [14]. Based on a recent fNIRS study on bimanual motor learning using oxygenated hemoglobin as the primary metric due to superior contrast-to-noise ratios [15], we postulated for our bipedal standing balance learning task that unskilled to skilled task performance could be related to the shift in the brain activation from the prefrontal cortex (PFC) to the sensorimotor cortex (SMC). Here, it is important to also investigate the neurovascular coupling with simultaneous fNIRS and EEG [16] since a reduction in PFC activation based on fNIRS oxygenated hemoglobin can also be due to tDCS facilitated neural efficiency; i.e., an increased neuronal performance negatively modulated increases in hemodynamic activity [17, 18].

Cerebellar brain inhibition (CBI) can show the recruitment of the cerebellar-M1 connections depending on the ctDCS polarity [19], which can be probed with paired-pulse transcranial magnetic stimulation (TMS) based on the CBI recruitment curve [19, 20]. We investigated the effects of ctDCS on the CBI recruitment curve in healthy humans [19], informed by the computational modeling of the electric field distribution in the cerebellum [21]. We found that both anodal and cathodal ctDCS significantly decreased CBI, where the recruitment varied depending on the ctDCS polarity and the cerebellar TMS intensity used for the CBI evaluation. This variability in the recruitment was postulated due to diverse effects on different cerebellar cell populations; therefore, we optimized the lobule-specific electric field distribution using our cerebellar lobules optimal stimulation (CLOS) pipeline [21] for ctDCS of the dentate nucleus and the lower-limb representations in the cerebellum [22]. Offline ctDCS as a priming intervention was found in our prior works to facilitate standing balance function in chronic stroke survivors during a challenging functional reach task in virtual reality (VR) [22] using an adaptive balance training platform [23] for operant conditioning (with reward-based feedback) [24]. Although paired-pulse TMS provided a rational approach to probe the cerebellar-M1 connections in our prior work [19], however, it was found challenging to perform in the rehabilitation setting. Moreover, ctDCS effects on the cerebellar-prefrontal connectivity cannot be probed with CBI due to the absence of motor-evoked potentials. Since TMS-based CBI evaluation is time-consuming and challenging to perform in a clinical rehabilitation setting, so, portable neuroimaging, including fNIRS-EEG imaging [16, 25, 26], needs further investigation. In principal accordance, the overarching aim of this methodological study was to investigate the feasibility of fNIRS-EEG joint-imaging of remote cerebral effects of focal ctDCS in identifying chronic post-stroke responders. The ctDCS electric field was kept limited to the cerebellum based on computational modeling [21], and the post-stroke responders were found based on behavioral measures from prior works [22, 27].

Zandvliet and colleagues [13] found that contra-lesional anodal ctDCS during the tracking task improved the standing balance performance in a tandem stance position in chronic stroke survivors but not in age-matched healthy controls. Zandvliet and colleagues [13] postulated that anodal ctDCS of the contra-lesional cerebellar hemisphere could strengthen the cerebellar—primary motor cortex (M1) connections to the

affected cortical hemisphere. However, Zandvliet and colleagues [13] did not present electric field distribution in the cerebellum, so the effects can be challenging to interpret without bilateral cerebellar lobule-specific (motor versus non-motor [28]) dose information. Zandvliet and colleagues [13] found that ipsilesional anodal ctDCS did not improve standing balance performance; however, the neurophysiological reason remained unknown since cerebellar brain inhibition was not measured, which may be necessary for elderly subjects [29]. In the current study, computational modeling [21] was used to identify two bipolar ctDCS montages from our related prior works [22, 27]. Our previous work [30] showed that anodal ctDCS of the anterior lobe of the cerebellum during visuomotor learning of myoelectric visual pursuit using electromyogram (EMG) from gastrocnemius muscle resulted in a statistically significant ($p<0.05$) decrease in the reaction time ("motor" loop effect?) post-intervention than baseline when compared to anodal ctDCS of the posterior lobe of the cerebellum as well as anodal ctDCS of combined anterior and posterior lobes of the cerebellum; however, only anodal ctDCS of combined anterior and posterior lobes of cerebellum resulted in a significant decrease in root mean square error ("cognitive" loop effect?) post-intervention than in baseline. Also, ctDCS of dentate nuclei from related prior works [22, 27] resulted in electric field distribution over combined anterior and posterior lobes of the cerebellum that was selected as one of the bipolar ctDCS montages. The second bipolar ctDCS montage was selected from related prior works [22, 27] to target the posterior lobe of the cerebellum for bilateral leg lobules VIIb-IX ("motor" loop effect). This will avoid affecting the Crus I and II ("cognitive" loop effect) that have shown to have projections only to the prefrontal cortex by viral tracing studies in non-human primates [31]. Also, functional neuroimaging studies in humans, e.g., functional MRI (fMRI) [32], have shown that the cerebellum projects to the association areas (prefrontal areas, posterior parietal, and superior temporal, posterior parahippocampal and cingulate areas). Recent data-driven analysis of fMRI has elucidated motor (lobules I–VI; lobule VIII) and non-motor (lobules VI-Crus I; lobules Crus II–VIIB; lobules IX–X) attentional/executive as well as default mode regions of the cerebellar function [33]. Prior works have also shown that prefrontal, premotor, supplementary motor, and parietal cortex have been found involved with standing balance control in hemiplegic stroke patients [34], so ctDCS-evoked cerebrum activity via inhibitory Purkinje cells or excitatory dentate nuclei pathway to the cortex may facilitate standing balance besides lobule-specific effects on the local cerebellar circuits.

This methodological study was motivated by our prior works that have shown that various established ctDCS electrode montages affect different parts of the cerebellum [21]. Here, optimized ctDCS of dentate nuclei facilitated standing balance [22] and gait [27] performance in chronic stroke survivors where lobule-specific electric field strength was found related to the standing balance performance based on a generalized linear model. However, portable (fNIRS-EEG) neuroimaging of the ctDCS effects due to the cerebellar connections with the cerebrum was not presented in our prior works vis-à-vis lobule-specific electric field strength. In this methodological study on chronic post-stroke subjects, based on prior fMRI studies [33] and our preliminary results [30], we postulated that ctDCS of the combined anterior and posterior lobes of the cerebellum, including cerebellar hemispheric lobules Crus I–Crus II and the dentate nucleus [22], should modulate the cerebrum activity differently than ctDCS of the posterior lobes of the cerebellum consisting of the hemispheric lobules VIIb-IX only [24, 26]. We evaluated the feasibility of fNIRS-EEG joint-imaging in the chronic stroke survivors (without cerebellar lesion) at the point of care in a low-resource setting that is necessary for clinical translation of fNIRS-EEG guided individualized dosing [35] of ctDCS in a home setting

## Materials and Methods

### Subjects and Their Age-Appropriate Head Modeling for Deep ctDCS

A convenience sample of a total of 14 male chronic (>6 months post-stroke) ischemic stroke subjects volunteered for the study. The hemiplegic subjects, who (i) were aged between 18 and 90 years, (ii) could walk independently for at least 10 m, (iii) could provide informed, and written consent, and (iv) could understand instruction from the experimenter, were enrolled. We then selected chronic stroke survivors with cerebral lesions but with an intact cerebellum (clinical notes based on computerized tomography, CT, scan at the stroke onset) so that the focal ctDCS electric field effects can be delivered to the cerebrum via the cerebellum [36]. Out of these 14 male volunteers, one (P13) could not complete the study because of his unavailability after initial screening, and the other (P14) was excluded from the study based on the exclusion criteria. Table 1 lists all the 12 male chronic stroke subjects (P1-P12, Mean (SD) = 46(±13) years) who participated in the current study. The physiotherapist administered the Berg Balance Scale [37] and ensured that the inclusion criteria were satisfied. Two subjects (P4, P5) had upper-limb ideomotor apraxia (based on imitation of hand gestures) but satisfied our inclusion criteria for the lower-limb study. Written informed consent was obtained from each subject, and the multi-center research protocol for this study was approved by the All India Institute of Medical Sciences, New Delhi, India Institutional Review Board, IRB, (IEC-129/07.04.2017), and Indian Institute of Technology Gandhinagar, India Institutional Review Board (IEC/2019-

**Table 1** Subject characteristics (all male) and subject-specific bipolar ctDCS (P4, P5 subjects have ideomotor apraxia)

| Name | Age and age-group (years) | Height (cm) | Weight (kg) | Berg balance scale | Post stroke period (years) | Hemiplegic side | Bilateral leg lobules VII–IX (anode-cathode) | Dentate nuclei (anode-cathode) |
|---|---|---|---|---|---|---|---|---|
| P1 | 44 (40–44) | 167 | 73 | 52 | 2 | Right | Exx8-Exx7 | PO10h-PO9h |
| P2 | 53 (50–54) | 171 | 70 | 43 | 3 | Right | Exx8-Exx7 | PO10h-PO9h |
| P3 | 40 (40–44) | 180 | 60 | 41 | 1 | Left | Exx7-Exx8 | PO9h-PO10h |
| P4 | 38 (35–39) | 165 | 80 | 52 | 1 | Right | Exx8-Exx7 | PO10h-PO9h |
| P5 | 32 (30–34) | 176 | 94 | 49 | 1 | Right | Exx8-Exx7 | PO10h-PO9h |
| P6 | 50 (50–54) | 162 | 60 | 50 | 2 | Left | Exx7-Exx8 | PO9h-PO10h |
| P7 | 61 (60–64) | 167 | 83 | 46 | 1 | Right | Exx7-Exx8 | PO9h-PO10h |
| P8 | 75 (70–74) | 163 | 76 | 41 | 6 | Right | Exx8-Exx7 | PO10h-PO9h |
| P9 | 45 (45–49) | 164 | 60 | 55 | 3 | Right | Exx8_Exx7 | PO10h-PO9h |
| P10 | 49 (45–49) | 167 | 70 | 55 | 2 | Left | Exx7-Exx8 | PO9h-PO10h |
| P11 | 54 (50–54) | 161 | 47 | 55 | 3 | Left | Exx8-Exx7 | PO10h-PO9h |
| P12 | 38 (35–39) | 165 | 76 | 55 | 2 | Right | Exx8-Exx7 | PO10h-PO9h |

20/4/UL/046). IRB approval was not available for the MRI/CT scans.

## Computational Head Modeling and Flatmap Visualization

Computational head modeling (details provided in Zeynab et al. [22]) was performed using an age-appropriate averaged ($n$ = 73) human brain MRI template for the relevant age-groups (see Table 1) that were obtained online at the https://jerlab.sc.edu/projects/neurodevelopmental-mri-database/ with the permission of Dr. John Richards. The human brain MRI template of subjects was all normal healthy adults with no history of neurological or psychiatric illness, head trauma with loss of consciousness, current or past use of psychostimulant medications, cardiovascular disease, and no abnormal findings the MRI [38]. Neurodevelopmental MRI database [38] consisted of average (male and female) T1-weighted MRI for the head across different age groups as well as the segmentation priors for gray matter (GM), white matter (WM), and cerebrospinal fluid (CSF), which was used for head modeling in CLOS pipeline [21]. In the CLOS pipeline, tetrahedral volume mesh was created using the ROAST toolbox [39], which is a Matlab (MathWorks, MA, USA) script based on three open-source software; Statistical Parametric Mapping (SPM) [40], Iso2mesh [41], and getDP [42]. ROAST used SPM12 to segment the head and the brain. After SPM12 segmentation and manual comparison with the segmentation priors from the neurodevelopmental MRI database [38], five tissues were labeled for the tetrahedral volume mesh, namely scalp, skull, CSF, GM, and WM. These different brain tissues for the volume mesh were modeled as different volume conductors during finite element analysis (FEA) in the ROAST. Here, isotropic conductivity based on prior works was used for different brain tissues [43], which were (in S/m) scalp = 0.465; skull = 0.01; CSF = 1.654; GM = 0.276; and WM = 0.126. In all the simulations, the voxel size was 1 $mm^3$.

Computational modeling of the cerebellar lobule-specific electric field distribution was performed for two bipolar ctDCS montages optimized in our prior work to focally target the dentate nuclei and the bilateral leg lobules VIIb-IX [22]. We postulated based on Zandvliet and colleagues [13] that anodal ctDCS of the contra-lesional cerebellar hemisphere could strengthen the cerebellar—cerebral connections to the affected cortical hemisphere. Our optimized bipolar ctDCS electrode montages were limited to the scalp overlying cerebellum so that they focally stimulated the cerebellar lobules without spillover to non-cerebellar regions, which was a problem in the case of the extracephalic electrode [22]. To investigate the electric field distribution in the cerebellar lobules, we extracted the electric field distribution within cerebellar white and gray matter [21]. The electric field was extracted using the CLOS pipeline [21] using the cerebellar masks of each head model assessed with the spatially unbiased atlas template (SUIT) toolbox [44]. We defined the parcellation of the cerebellar regions according to the SUIT atlas [44]. The cerebellar maps were visually inspected in image viewer software by the first author. The 2D representation of electric field distribution and the visualization of electric field distribution across the cerebellar volume for all patients were implemented using the flatmap script in the SUIT toolbox [44].

(1) *Bipolar PO9h – PO10h montage for dentate nuclei:* A 3.14$cm^2$ (1-cm radius) circular anode was placed at the contra-lesional side, a 3.14$cm^2$ cathode was placed at the ipsilesional side for ctDCS with 2-mA direct current.

(2) *Bipolar Exx7 – Exx8 montage for bilateral leg lobules VIIb-IX:* A 3.14cm$^2$ (1-cm radius) circular anode was placed at the contra-lesional side, a 3.14cm$^2$ cathode was placed at the ipsilesional side for ctDCS with 2-mA direct current.

## Experimental Study Protocol

At the start of the study session, the subjects were asked to sit and relax for about 5 min. Then, the experimenter explained to the subject what they were expected to do in the study that required a commitment of about an hour. The two optimized ctDCS montages, Bipolar PO9h – PO10h and Bipolar Exx7 – Exx8 (see "Computational Head Modeling and Flatmap Visualization" section for details), were applied to the 12 male chronic stroke subjects in random order to counterbalance in a cross-over repeated measure single-blind experimental design with a washout period of at least 2 days. The experimenter prepared the subject by placing an fNIRS-EEG/tDCS STARSTIM 8 (Neuroelectrics, Spain) cap with both the electrode montages on the subject's head. Then, 2 min of baseline resting-state fNIRS-EEG data were collected that was found sufficient for functional connectivity analysis [45, 46]. Then, the subjects performed virtual reality (VR)–based balance training (VBaT) [23] for about 10 min. During VBaT, subjects had to shift the body weight in different directions (North, South, East, West, etc.) using an ankle strategy based on the VBaT platform's cues [23]. The VBaT tasks required the subjects to maneuver different virtual objects in the VR environment using their center of pressure (CoP) while performing weight shifting on a Wii balance board (WiiBB), and then maintaining their posture to hold the virtual objects at target locations in the VR space [23]. The CoP values were acquired from WiiBB at 30 Hz and were preprocessed by a 5-point moving average filter before modulating the virtual objects in the VR environment. VBaT provided the subjects with audio-visual feedback on successfully reaching the target using CoP. After VBaT tasks, the subject was asked to sit and relax on a chair when 2 min of fNIRS-EEG data were collected. Subsequently, bipolar ctDCS was delivered for 15 min in the seated resting position with a current intensity of 2 mA via 3.14 cm$^2$ Pistim (Neuroelectrics, Spain) electrodes that were also used for EEG monitoring (not during ctDCS). Following this, 2 min of post-tDCS fNIRS-EEG data were collected before the subject repeated VBaT tasks, followed by another 2 min of fNIRS-EEG recording in the resting-state. Therefore, the fNIRS-EEG data were recorded in continuous epochs of 30 s for 2 min before and after VBaT tasks, which were conducted before (pre-intervention) and after (post-intervention) 15 minutes of bipolar ctDCS. Figure 1 shows the experimental setup and the protocol.

## Simultaneous Functional Near-Infrared Spectroscopy and Electroencephalography of the ctDCS Response

The fNIRS-EEG portable neuroimaging and triaxial accelerometry (at 100 S/s) were conducted using a wireless simultaneous fNIRS-EEG imaging system that used the lab streaming layer (LSL) for time-synchronization. STARSTIM fNIRS-EEG system combined a wireless STARSTIM 8 stimulator (Neuroelectrics, Spain) for 8-channel tDCS and EEG in conjunction with fNIRS using OctaMon+ system (Artinis, Netherlands). The fNIRS montage targeted cerebral regions, including the prefrontal cortex (Brodmann areas 8, 9, and 46) and sensorimotor cortex (Brodmann areas 1, 2, 3, and 4), based on prior fMRI studies [47] that showed that the prefrontal cortex (PFC) regions are functionally connected to multiple regions of the human cerebellum, e.g., Crus I with medial prefrontal cortex (MPFC), Crus II with dorsolateral prefrontal cortex (DLPFC), while dorsal lobule VI and ventral VIIB–VIIIA with anterior prefrontal cortex (APFC). In AtlasViewer, left MPFC is −12, 48, 20 and right MPFC is 12, 48, 20; left DLPFC is −42, 16, 36 and right DLPFC is 42, 16, 36; and left APFC is −32, 40, 28 and right APFC is 32, 40, 28, in the MNI coordinate system (x, y, z). Prior work [48] has also shown that the sensorimotor cortex, SMC (Brodmann areas 1, 2, 3, and 4), including the premotor cortex, supplementary motor area (SMA), the primary motor cortex (M1), and parietal cortex, are characterized by the sensorimotor rhythm, typically at a frequency of 8–13 Hz that can be affected with ctDCS. Therefore, the 8-channel EEG was recorded from Fp1, Fp2, F3, F4, C3, C4, P3, and P4 scalp locations (10–20 positioning system). The eight fNIRS sources were positioned at AF7, AF3, AF8, AF4, CP4, FC4, CP3, and FC3, and the two fNIRS detectors were placed at the Cz and FPz with a source-detector distance of around 35mm. Computational head modeling for fNIRS sensitivity analysis was performed with an age-appropriate averaged human brain MRI template. Sensitivity analysis was performed for the fNIRS montage consisting of 8 sources and two detectors using Monte Carlo simulation that provided a probabilistic model of the path of the photons. The Monte Carlo simulation generated a forward matrix that represented each channel's spatial sensitivity profile (source-detector pair) to the cortical absorption changes. Here, the sensitivity analysis was performed using the AtlasViewer toolbox [49], a toolbox for the determination of brain coordinates and the sensitivity measurement for the source-detector montages. The AtlasViewer toolbox facilitates the optimal placement of the optodes or probes for the fNIRS studies. The probes were first designed in AtlasViewer with the eight sources placed at AF7, AF3, AF8, AF4, CP4, FC4, CP3, and FC3, and the two detectors at Cz and FPz. The probe design was then registered to the individual head model's surface, followed by the projection to the cortex. This projection to the cortex, found by drawing

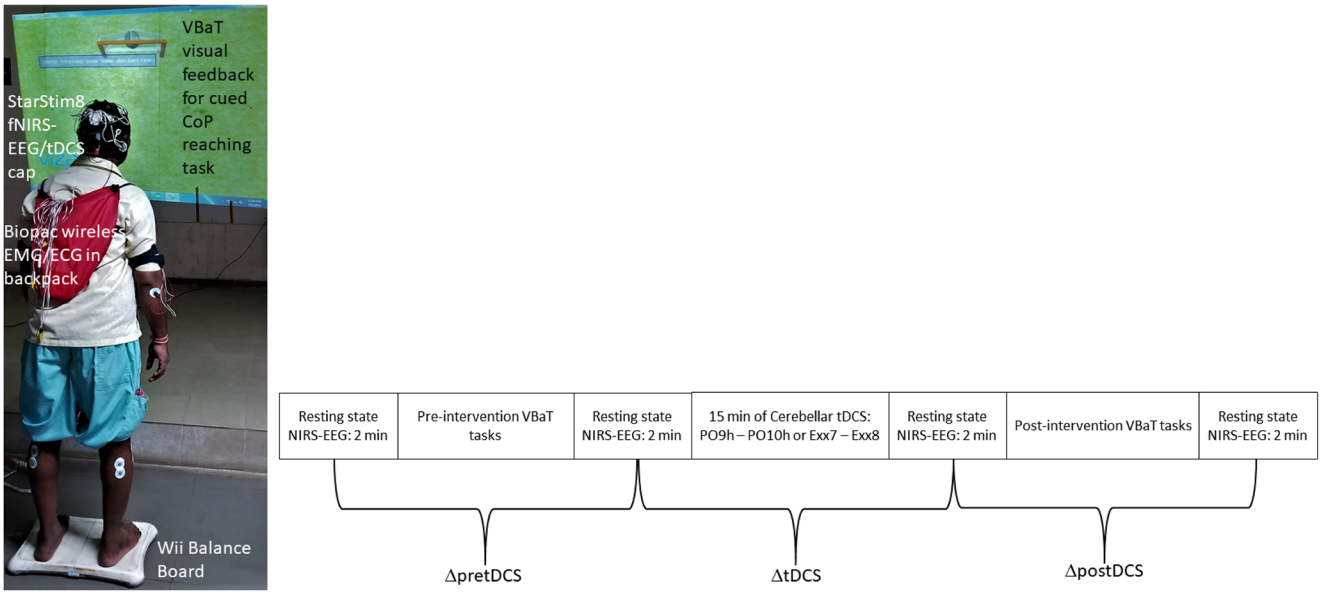


**Fig. 1** Left panel: Experimental setup for ctDCS facilitated virtual reality (VR)–based balance training (VBaT). Right panel: experimental protocol—resting-state fNIRS-EEG data was collected for 2 min before and after the measures of virtual reality–based balance training (VBaT) before (pre-intervention) as well as after (post-intervention) 15 minutes of cerebellar anodal tDCS using two bipolar montages (PO9h – PO10h or Exx7 – Exx8) on 12 stroke survivors using a counterbalanced cross-over repeated measures experimental design

vectors perpendicular to the surface at the midpoint of each source-detector pair, ensured the sensitivity to the broad brain regions, including the PFC (Brodmann areas 8, 9, and 46) and SMC (Brodmann areas 1, 2, 3, and 4). The Monte Carlo simulation was set up with 100 million photons being injected by each source using the default optical parameters for each layer of the head model. The sensitivity profile is shown in Figure S1 (in Supplementary material) with the voxel size of 1 $mm^3$. In this methodological study, we investigated the feasibility of capturing ctDCS effects on the relation between the latent variables (from canonical correlation analysis) for the fNIRS and EEG signals [50].

## Simultaneous Functional Near-Infrared Spectroscopy and Electroencephalography in the Latent Canonical Space

The resting-state fNIRS-EEG data before and after VBaT were preprocessed with the HOMER3 (https://github.com/BUNPC/Homer3) and the EEGLAB toolbox in Matlab (MathWorks, Inc. USA). EEG data was first down-sampled to 250 Hz and then was de-trended by high-pass filtering with a 1-Hz cutoff frequency. Line noise and its harmonics were removed using "CleanLine," and then EEG data were re-referenced to the common average. Then, the continuous EEG data were processed with artifact subspace reconstruction (ASR) [51], and then the adaptive mixture independent component analysis (AMICA) was performed in EEGlab [52]. The artifactual components were removed by IClabel [53] and visual inspection [54], which made the fNIRS-EEG data discontinuous with the discontinuity marked as events in the EEGlab. We used HOMER3 routines in Matlab (MathWorks, Inc.) for the fNIRS data analysis based on the modified Beer-Lambert law to find the changes in the oxy-hemoglobin (O2Hb) and deoxy-hemoglobin (HHb) concentrations. One of the challenges is a high sensitivity for the scalp and other extracranial hemodynamics, including changes in the heartbeat and the breathing cycle, that can mask cerebral activation [55]. Usually, more significant changes are observed in the extracranial O2Hb when compared to extracranial HHb concentration. First, channels with low scalp coupling were identified based on the PHOEBE approach [56] that flagged most fNIRS data during VBaT tasks. Although one can apply the HOMER3 method (https://github.com/avolu/tCCA-GLM) proposed by Luhmann et al. [57] using synchronized triaxial accelerometer data (from STARSTIM 8) to reduce the movement artifacts, in this study, we discarded all the fNIRS-EEG data during VBaT tasks due to possible detrimental effects of co-modulated movement artifacts on the canonical correlation analysis. Subsequently, we performed the principal component analysis to remove the first principal component representing the global covariance due to the extracranial hemodynamic signals [58]. Thereafter, we performed band-pass in two frequency bands, vasomotion band (0.07–0.13 Hz) and neurovascular coupling band (0.01–0.07Hz) [59], with zero-lag Butterworth filtering to remove the heart rate, respiratory rate, and other high- and low-frequency noise. After preprocessing the fNIRS-EEG data in the EEGlab and HOMER3, we identified four epochs of

continuous 30 s of resting-state fNIRS-EEG data (using the discontinuity event markers) before and after VBaT tasks.

A total of 4 groups of 2 min of fNIRS-EEG data were recorded in the resting state conditions before and after the VBaT task, which was performed before and after the bipolar ctDCS intervention (see Fig. 1 for the experimental study protocol). Therefore, fNIRS-EEG signal changes (i.e., $\frac{(\text{PostMean}-\text{PreMean})}{(\text{PostMean}+\text{PreMean})}$) could be measured before and after the VBaT task, before the ctDCS intervention (called (ΔpretDCS), then, from before and after the ctDCS intervention (called ΔtDCS), and also, from before and after the VBaT task after the ctDCS intervention (called ΔpostDCS). Based on our prior work [8], we evaluated the coupling between the log10-transformed EEG bandpower within 1–45 Hz, and the total hemoglobin (tHb=O2Hb+HHb) signals within the 0.07–0.13Hz based on canonical correlation analysis. We also performed canonical correlation analysis between the log10-transformed EEG bandpower within 1–45 Hz and the tHb signals within the 0.01–0.07-Hz band. Here, the log10-transformed EEG bandpower within 1–45Hz covered the five EEG frequency bands: δ (1–4 Hz), θ (4–7Hz), α (7–13 Hz), β (13–30 Hz), and γ (30–45 Hz) that contained most of the total EEG power related to the metabolic cost of the neural activity [60]. Then, temporally embedded canonical correlation analysis (tCCA) was applied separately to the fNIRS-EEG resting-state data from the four regions of interests (ROIs), namely the left and the right prefrontal cortex (PFC) (fNIRS—left: AF3-FPz, AF7-FPz; right: AF4-FPz, AF8-FPz, and EEG—left: Fp1, F3; right Fp2, F4) and the left and the right sensorimotor cortex (SMC) (fNIRS—left: CP3-Cz, FC3-Cz; right: CP4-Cz, FC4-Cz, and EEG—left: C3, P3; right C4, P4). Here, tCCA maximized the correlation between the log10-transformed EEG bandpower and fNIRS tHb time-series (0.01–0.07Hz and 0.07–0.13Hz bands) across all the channels of an ROI to identify the latent variables (or, canonical scores) where Wilks' lambda (likelihood ratio) statistic (>0.95) was used to test the null hypothesis that the canonical correlations are zero. Also, canonical scores for fNIRS O2Hb and HHb signal and the log10-transformed EEG bandpower under tCCA of an ROI were used to indicate the change in the brain activation at that ROI (left PFC, right PFC, left SMC, right SMC). Here, the canonical scores for fNIRS O2Hb and HHb signal in the latent space are postulated to be less sensitive to the systemic artifacts than the fNIRS O2Hb and HHb signals themselves. We also performed an analysis of variance (ANOVA) to test the effects of the factors, brain location (ROIs), ctDCS montage, and state (ΔpretDCS, ΔtDCS, ΔpostDCS), on the changes (i.e., $\frac{(\text{PostMean}-\text{PreMean})}{(\text{PostMean}+\text{PreMean})}$) in the canonical correlation and the canonical scores at a 5% significance level across all the subjects.

### Multivariate General Linear Model with Lobular Electric Field Distribution as the Predictor and fNIRS-EEG Brain Activations as the Response Variables

We investigated the effects of the lobular electric field distribution (independent variables) in the cerebellum from focal ctDCS [22] on the changes (i.e., $\Delta\text{tDCS} = \frac{(\text{PostMean}-\text{PreMean})}{(\text{PostMean}+\text{PreMean})}$) in brain activation measures (dependent variables) using a multivariate general linear model (GLM) across subjects. The following changes in the brain activations (dependent variables) were measured in the resting-state at the left and the right PFC and SMC locations (four ROIs) that were related to the ipsilesional (Ipsi) and contra-lesional (Contra) hemispheres in stroke survivors: canonical scores for fNIRS O2Hb, fNIRS HHb, and log10-transformed EEG bandpower signal after tCCA. The average strength of the electric field (independent variables) in the following cerebellar locations were based on age-specific computational modeling [21] using ipsi-lesional (Ipsi) and contra-lesional (Contra) SUIT labels: "Ipsi I-IV," "Contra I-IV," "Ipsi V," "Contra V," "Ipsi VI," "Vermis VI," "Contra VI," "Ipsi Crus I," "Vermis Crus I," "Contra Crus I," "Ipsi Crus II," "Vermis Crus II," "Contra Crus II," "Ipsi VIIb," "Vermis VIIb," "Contra VIIb," "Ipsi VIIIa," "Vermis VIIIa," "Contra VIIIa," "Ipsi VIIIb," "Vermis VIIIb," "Contra VIIIb," "Ipsi IX," "Vermis IX," "Contra IX," "Ipsi X," "Vermis X," "Contra X," "Ipsi Dentate," "Contra Dentate," "Ipsi Interposed," "Contra Interposed," "Ipsi Fastigial", "Contra Fastigial," and "Non-Cerebellar Brain." Due to multicollinearity and singularity in the lobular average electric field strengths across subjects as independent variables, principal component analysis (PCA) was conducted to identify principal components (PCs) that accounted for greater than 98% variance across subjects. Therefore, in principal component regression, a multivariate GLM ("mvregress" in Matlab) was fitted to the PCs of the mean lobular electric field strength as the predictor and the brain's latent variables of activation as the response across all the subjects.

## Results

### Computational Head Modeling

We investigated the 3D lobular electric field distribution using 2D visualization in SUIT flatmap—see Fig. 2a. This 2D visualization was for our two ctDCS electrode montages (one-size-fits-all), shown in Fig. 2b, where the SUIT flatmap is shown in Fig. 2c for all the twelve subjects. In Fig. 2c, the results for the bipolar PO9h – PO10h montage for dentate nuclei are shown in the right column, and the results for the bipolar Exx7 – Exx8 montage for bilateral leg lobules VIIb-IX are shown in the left column. The maximum electric field strength varied across subjects due to differences in their age

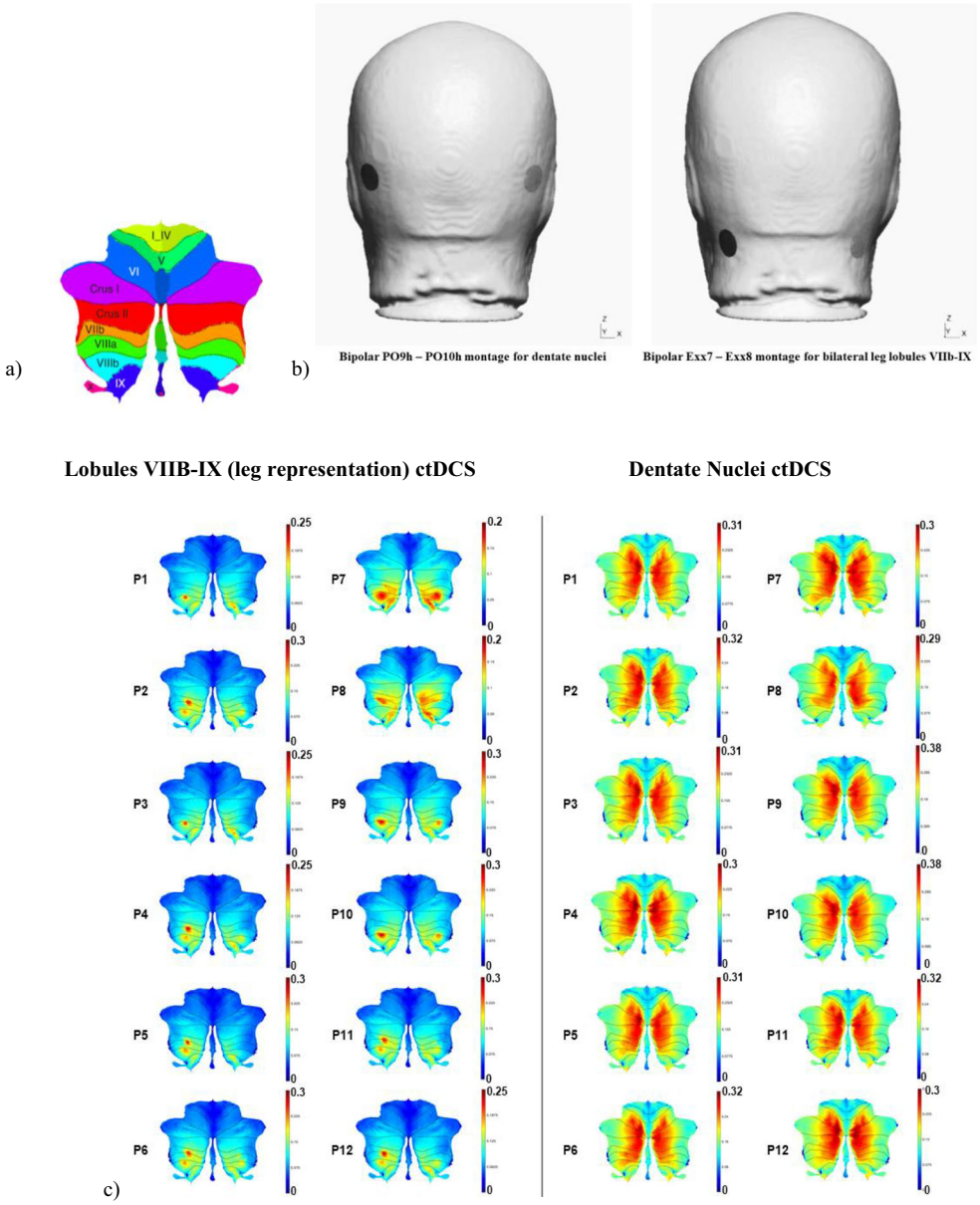


**Fig. 2** **a** 2D representation of the 28 cerebellar lobules using SUIT flatmap. **b** Two ctDCS electrode montages, namely, Bipolar PO9h – PO10h montage for dentate nuclei, where a 1-cm radius circular anode was placed at the contra-lesional side, and a 1-cm radius circular cathode was placed at the ipsi-lesional side for ctDCS with 2mA direct current, and Bipolar Exx7 – Exx8 montage for bilateral leg lobules VIIb-IX where a 1-cm radius circular anode was placed at the contra-lesional side, and a 1-cm radius circular cathode was placed at the ipsi-lesional side for ctDCS with 2-mA direct current. **c** Electric field strength (V/m) across different subjects using SUIT flatmap (SUIT toolbox) with the color scale representing the electric field strength shown on the right. The left two columns show the electric field distribution that resulted from the bipolar Exx7 – Exx8 montage for bilateral leg lobules VIIb-IX, while the right two columns present the results for the bipolar PO9h – PO10h montage for dentate nuclei

groups for these one-size-fits-all ctDCS montages. Nevertheless, the bipolar PO9h – PO10h montage for dentate nuclei was found to affect both the anterior and posterior lobes of the cerebellum (including Crus I–Crus II), while the bipolar Exx7 – Exx8 montage for bilateral leg lobules VIIb-IX primarily affected the posterior lobes of the cerebellum (excluding Crus I–Crus II).

## Canonical Correlation Analysis of Resting-State Functional Near-Infrared Spectroscopy and Electroencephalography Signals

Canonical correlation analysis was only feasible between the log10-transformed EEG bandpower within 1–45Hz, and the tHb signals within the 0.07–0.13-Hz frequency band based on Wilks' lambda statistic (<0.95). Boxplots of the effects of the factors, brain location (ROIs), ctDCS montage, and the state (ΔpretDCS, ΔtDCS, ΔpostDCS), on the canonical scores of O2Hb are shown in Fig. 3a and on the canonical scores of log10-transformed EEG bandpower are shown in Fig. 3c. Here, the central mark indicates the median, and the bottom and top edges of the box indicate the 25th and 75th percentiles, respectively. The whiskers extend to the most extreme data points not considered outliers, and the outliers are plotted individually using the "+" symbol. Three-way ANOVA test on the effects of the factors, brain location (ROIs), ctDCS montage, and the state (ΔpretDCS, ΔtDCS, ΔpostDCS), showed a moderate but non-significant ($p$=0.0788) interaction effect between the ctDCS montage and the state on canonical scores of O2Hb, as shown in the left panel of Fig. 3b. The

interaction plot shown in the right panel of Fig. 3b is a matrix plot that displays the interaction between the grouping variables or factors, with the number of rows and columns equal to the number of factors. For interaction between the ctDCS montage and the state on canonical scores of O2Hb ($p$=0.0788), the bipolar PO9h – PO10h montage for dentate nuclei was found to increase the canonical scores of O2Hb while the bipolar Exx7 – Exx8 montage for bilateral leg lobules VIIb-IX was found to decrease the canonical scores of O2Hb. The canonical scores of O2Hb decreased after the VBaT tasks, both before (pre-intervention) as well as after (post-intervention) ctDCS intervention (both montages). A significant effect of the state ($p$=0.0019) and an interaction between the ctDCS montage and the state ($p$=0.0153) were found for the canonical scores of log10-transformed EEG bandpower, as shown in the left panel of Fig. 3d. The interaction plot shown in the right panel of Fig. 3c reveals that both the ctDCS montages increased the canonical scores of log10-transformed EEG bandpower while VBaT decreased the same before (pre-intervention) as well as after (post-intervention) ctDCS intervention (both montages).

Boxplots of the canonical correlations and the canonical scores of HHb are shown in Fig. 4, where the central mark indicates the median, and the bottom and top edges of the box indicate the 25th and 75th percentiles, respectively. The whiskers extend to the most extreme data points not considered outliers, and the outliers are plotted individually using the "+" symbol. Three-way ANOVA results on the effects of the factors, brain location (ROIs), ctDCS montage, and the state (ΔpretDCS, ΔtDCS, ΔpostDCS), showed no significant effects on the canonical correlations and the canonical scores of HHb at a 5% significance level.

### Multivariate General Linear Modeling

To understand the hierarchical binary cluster tree of the mean lobular electric field strength for the two ctDCS montages across subjects, we performed hierarchical clustering based on the average Euclidean distance (i.e., lobules having similar mean lobular electric field strength will be clustered together) and showed that as *dendrogram* plot (or, hierarchical cluster tree) in Fig. 5a. The *dendrogram* plot consists of many U-shaped lines that connected the 30 clusters (total 30 from SUIT without the "Ipsi Interposed," "Contra Interposed," "Ipsi Fastigial," "Contra Fastigial," "Non-Cerebellar Brain") of mean lobular electric field strength where the height of each U represented the Euclidean distance between the two clusters that are connected. In the *dendrogram* plot, the dentate nuclei formed a separate binary cluster based on Euclidean distance (in $y$-axis), shown in blue in Fig. 5a. The other binary clusters can then be further divided into two clusters based on Euclidean distance (in $y$-axis), shown in red and green in Fig. 5a, which represented the similarity of the mean lobular electric field strength across those lobules (x-axis). Therefore, the two ctDCS montages from our prior work [22] differentiated the mean lobular electric field strength at the dentate nuclei from that at the other lobules of the cerebellum even with a "one-size-fits-all" approach in our stroke survivors across a wide age range (32–75 years).

Principal component analysis of the mean lobular electric field strength for the two ctDCS montages across subjects led to two principal components (PCs) that together accounted for greater than 98% variance (VAF). Here, the first PC (PC1) accounted for 97.5% variance that can be used as the sole predictor with VAF= 97.5% for the multivariate GLM. Figure 5b shows the PC1 of the mean lobular electric field strength as the predictor and the latent variable of the O2Hb as the response variable (left panel) along with its standardized residuals (right panel). Here, for the regression model shown in the left panel of Fig. 5b, $\text{ipsiPFC} = 0.0128 + 0.0554 \times \text{PC1} - 0.0783 \times \text{PC2}$; $\text{contPFC} = 0.0079 + 0.0758 \times \text{PC1} - 0.0085 \times \text{PC2}$; $\text{ipsiSMC} = -0.0056 - 0.0199 \times \text{PC1} - 0.2011 \times \text{PC2}$; $\text{contSMC} = -0.0068 + 0.0075 \times \text{PC1} - 0.3394 \times \text{PC2}$. Figure 5c shows the first PC (PC1) of the mean lobular electric field strength (VAF= 97.5%) as the predictor and the latent variable of the log10-transformed EEG bandpower as the response variable (left panel) along with its standardized residuals (right panel). Here, for the regression model shown in the left panel of Fig. 5c, $\text{ipsiPFC} = 0.0074 - 0.0228 \times \text{PC1} - 0.0910 \times \text{PC2}$; $\text{contPFC} = 0.0075 - 0.0001 \times \text{PC1} + 0.0370 \times \text{PC2}$; $\text{ipsiSMC} = 0.0051 + 0.0019 \times \text{PC1} - 0.2558 \times \text{PC2}$; $\text{contSMC} = -0.0021 - 0.0023 \times \text{PC1} + 0.0120 \times \text{PC2}$. In our 2D space defined by PC1 and PC2, the standardized residuals should have a bivariate standard normal distribution which is shown with an overlay in the right panel of Fig. 5b and c. Here, both the standardized residual plots show a bivariate standard normal distribution with little evidence against the multivariate normality assumption.

## Discussion

We presented the feasibility of fNIRS-EEG joint-imaging of the ctDCS effects on cerebral activation in chronic stroke survivors where a moderate but non-significant ($p$=0.0788) interaction between the ctDCS montage and the state (ΔpretDCS, ΔtDCS, ΔpostDCS) on the canonical scores of O2Hb was found—see Fig. 3b. However, a significant effect of the state ($p$=0.0019), as well as an interaction between the ctDCS montage and the state ($p$=0.0153), was found for the canonical scores of log10-transformed EEG bandpower—see Fig. 3d. No significant ctDCS effect on the canonical correlations was found even when the canonical correlations themselves were significant based on Wilks' lambda (likelihood ratio) statistic (>0.95). We investigated canonical correlations in both the vasomotion band (0.07–0.13Hz) and the

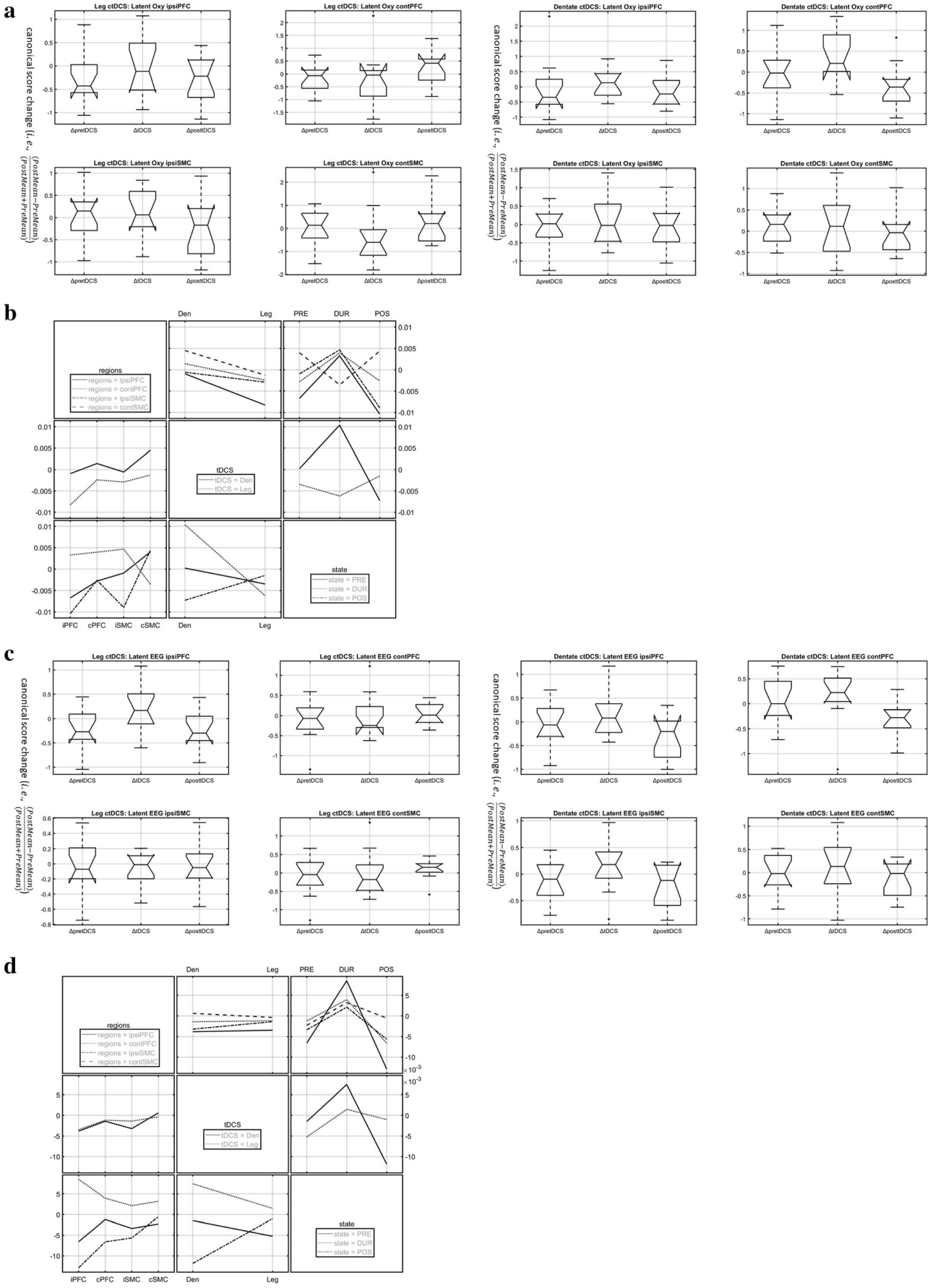
a
Leg ctDCS: Latent Oxy ipsiPFC
Leg ctDCS: Latent Oxy contPFC
Dentate ctDCS: Latent Oxy ipsiPFC
Dentate ctDCS: Latent Oxy contPFC
Leg ctDCS: Latent Oxy ipsiSMC
Leg ctDCS: Latent Oxy contSMC
Dentate ctDCS: Latent Oxy ipsiSMC
Dentate ctDCS: Latent Oxy contSMC
canonical score change (i.e., (PostMean−PreMean)/(PostMean+PreMean))
ΔpretDCS
ΔtDCS
ΔposttDCS
b
Den
Leg
PRE
DUR
POS
regions
regions = ipsiPFC
regions = contPFC
regions = ipsiSMC
regions = contSMC
tDCS
tDCS = Den
tDCS = Leg
state
state = PRE
state = DUR
state = POS
iPFC
cPFC
iSMC
cSMC
c
Leg ctDCS: Latent EEG ipsiPFC
Leg ctDCS: Latent EEG contPFC
Dentate ctDCS: Latent EEG ipsiPFC
Dentate ctDCS: Latent EEG contPFC
Leg ctDCS: Latent EEG ipsiSMC
Leg ctDCS: Latent EEG contSMC
Dentate ctDCS: Latent EEG ipsiSMC
Dentate ctDCS: Latent EEG contSMC
canonical score change (i.e., (PostMean−PreMean)/(PostMean+PreMean))
ΔpretDCS
ΔtDCS
ΔposttDCS
d
Den
Leg
PRE
DUR
POS
regions
regions = ipsiPFC
regions = contPFC
regions = ipsiSMC
regions = contSMC
tDCS
tDCS = Den
tDCS = Leg
state
state = PRE
state = DUR
state = POS
iPFC
cPFC
iSMC
cSMC

◀ **Fig. 3** Three-way ANOVA results shown along with the boxplots of the effects of the factors, brain location, ctDCS montage, and state (Δ*pretDCS*, Δ*tDCS*, Δ*postDCS*) as well as their interaction plots, on the canonical scores of O2Hb (Oxy, **a** and **b**) and the log10-transformed EEG bandpower (EEG, **c** and **d**). **a** Boxplot of the effects of the factors, brain location, ctDCS montage, and state (Δ*pretDCS*, Δ*tDCS*, Δ*postDCS*) of the canonical scores of O2Hb. On each box in the box plot, the central mark indicates the median, and the bottom and top edges of the box indicate the 25th and 75th percentiles, respectively. The whiskers extend to the most extreme data points not considered outliers, and the outliers are plotted individually using the *"+"* symbol. **b** Three-way ANOVA results (left panel) and the interaction plots (right panel) of the canonical scores of O2Hb for the factors, brain location (ipsilesional prefrontal cortex: ipsiPFC, contra-lesional prefrontal cortex: contPFC, ipsi-lesional sensorimotor cortex: ipsiSMC, contra-lesional sensorimotor cortex: contSMC), ctDCS montage (Dentate ctDCS: Den, Leg area ctDCS: Leg), and state (Δ*pretDCS* : *PRE*, Δ*tDCS* : *DUR*, Δ*postDCS* : *POS*). The interaction plot is a matrix plot, with the number of rows and columns both equal to the number of grouping variables or factors. **c** Boxplot of the effects of the factors, brain location, ctDCS montage, and state (Δ*pretDCS*, Δ*tDCS*, Δ*postDCS*) on the canonical scores of EEG bandpower. On each box in the box plot, the central mark indicates the median, and the bottom and top edges of the box indicate the 25th and 75th percentiles, respectively. The whiskers extend to the most extreme data points not considered outliers, and the outliers are plotted individually using the *"+"* symbol. **d** Three-way ANOVA results (left panel) and the interaction plots (right panel) on the canonical scores of EEG bandpower for the factors, brain location (ipsilesional prefrontal cortex: iPFC, contra-lesional prefrontal cortex: cPFC, ipsi-lesional sensorimotor cortex: iSMC, contra-lesional sensorimotor cortex: cSMC), ctDCS montage (Dentate ctDCS: Den, Leg area ctDCS: Leg), and state (Δ*pretDCS* : *PRE*, Δ*tDCS* : *DUR*, Δ*postDCS* : *POS*). The interaction plot is a matrix plot, with the number of rows and columns both equal to the number of grouping variables or factors

neurovascular coupling band (0.01–0.07Hz) [59] of fNIRS tHb, where only the vasomotion band provided significant canonical correlations based on Wilks' lambda (likelihood ratio) statistic (>0.95). We also performed principal component regression analysis on the lobular electric field distribution that showed PC1 (VAF=97.5%) representing the primary effect of the mean lobular electric field strength across subjects negatively correlated with the latent variables of the log10-transformed EEG bandpower at the contra-lesional PFC and SMC, and the ipsilesional PFC, while positively correlated with that at the ipsilesional SMC—see Fig. 5c. For the latent variables of the O2Hb, the PC1 (VAF= 97.5%) was positively correlated with the latent variables of the O2Hb at the contra-lesional PFC and SMC, the ipsilesional PFC, while negatively correlated with that for the ipsilesional SMC—see Fig. 5b. These results indicate a lobule-specific electric field effect across subjects on the cerebral activation that is postulated to be related to the cerebrocerebellar circuits or dysfunction thereof. In the current study, we used two different ctDCS montages where the bipolar PO9h – PO10h montage for dentate nuclei affected both the lobes of the cerebellum (including Crus I–Crus II) while the bipolar Exx7 – Exx8 montage for bilateral leg lobules VIIb-IX primarily affected the posterior lobes of the cerebellum (excluding Crus I–Crus II). To our knowledge, this is the first study reporting fNIRS-EEG-based measure of brain activations at the PFC and SMC that can be putatively associated with the lobular ctDCS electric field strength in the chronic stroke survivors that warrants a TMS-based neurophysiological validation in the future. VBaT was used to investigate standing balance function where CoP trajectories during cued weight shifts in different directions elucidated lower-limb ideomotor apraxia (IMA) in our post-stroke subjects with upper-limb IMA, which may contribute to patients' overall day-to-day motor disability [61]. VBaT tasks are goal-directed whole-body behavior using the CoP, where distinct neural circuits are responsible for the acquisition and performance of goal-directed behavior. Here, IMA can be related to cognitive deficits in declarative knowledge of manipulating CoP actions for performing the VBaT tasks.

We found an interaction effect between the ctDCS montage and the state (ΔpretDCS, ΔtDCS, ΔpostDCS) for the change in the canonical scores of O2Hb ($p$=0.0788) that indicated ctDCS modulation of the PFC and SMC activations evoked by VBaT tasks (i.e., ΔpretDCS, ΔpostDCS)—see Fig. 3b and d for the interaction plots. The effects of biped VBaT on the PFC and SMC activations can be interpreted based on prior works on bimanual motor skill acquisition that showed a decrease in the O2Hb activation of the PFC with increased practice [15]. Figure 3b shows the interaction plots for the canonical scores of O2Hb where a decrease at the contra-lesional SMC and an increase at both PFCs and ipsilesional SMC can be found due to ctDCS (i.e., ΔtDCS). We also found a decrease in the canonical score of O2Hb at both the PFCs and ipsilesional SMC while an increase at the contra-lesional SMC following first VBaT (i. e., ΔpretDCS) and second VBaT (i.e., ΔpostDCS) exposures to the novice post-stroke subjects—see Fig. 3b. Here, the difference in the responses at the bilateral SMCs can be related to inter-hemispheric inhibition where ctDCS of the bilateral leg lobules VIIb–IX was found to have a greater effect than the ctDCS of the dentate nuclei. During VBaT motor skill learning, the decrease in the activation at the PFCs (decreased "cognitive" load) with an increase in the activation at the contra-lesional (un-affected) SMC (increased "motor memory") may indicate the development of "motor memory" with "cognitive" learning [62]. We postulate that extended training on VBaT goal-directed tasks using CoP [24] can facilitate "automatizing" of the post-stroke standing balance function where practice will lessen the cognitive demand, shifting peak fNIRS-EEG activation from PFC to the dominant SMC.

Starting from the PFC, a cortical-dorsomedial striatal circuit is responsible for acquiring goal-directed actions while a cortical-ventral striatal circuit mediates the performance. Brain structures responsible for goal-directed behavior are

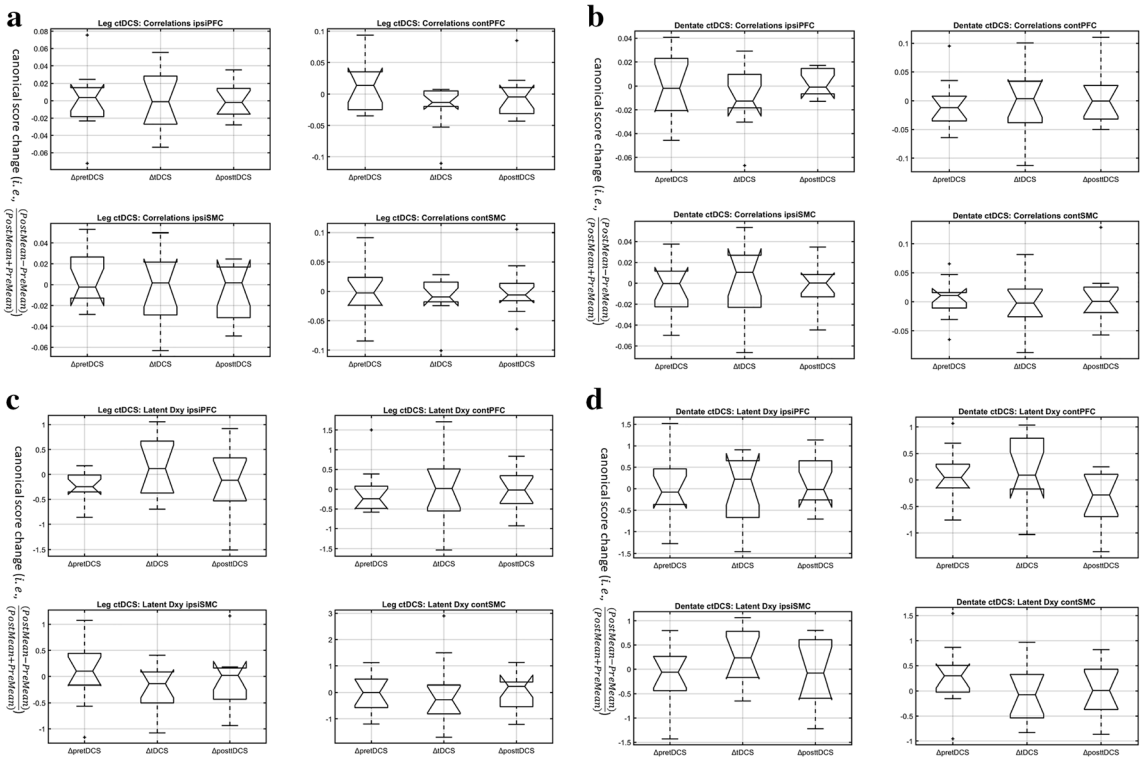


**Fig. 4** Boxplots of the effects of the factors, brain location (ipsilesional prefrontal cortex: ipsiPFC, contra-lesional prefrontal cortex: contPFC, ipsilesional sensorimotor cortex: ipsiSMC, contra-lesional sensorimotor cortex: contSMC), ctDCS montage (Dentate ctDCS: Den, Leg area ctDCS: Leg), ctDCS montage, and state ($\Delta pretDCS$, $\Delta tDCS$, $\Delta postDCS$), on the canonical scores of canonical correlations (*correlations*, **a** and **b**) and HHb (Dxy, **c** and **d**) was found insignificant at a 5% significance level in a three-way ANOVA test. On each box in the box plot, the central mark indicates the median, and the bottom and top edges of the box indicate the 25th and 75th percentiles, respectively. The whiskers extend to the most extreme data points not considered outliers, and the outliers are plotted individually using the *"+"* symbol

the medial prefrontal and orbitofrontal cortices, hippocampus, ventral, and dorsomedial striatum. In contrast, the sensorimotor cortices and dorsolateral striatum mediate the automatized/reflexive behavior in the experts. Here, the dorsomedial striatum (DMS) receives excitatory inputs from PFC, whereas the dorsolateral striatum (DLS) primarily receives inputs from the sensorimotor and premotor cortices. This mapping from the prefrontal and sensorimotor cortices is important since DMS and DLS activity patterns have been shown [63] to be distinct during early training. They are postulated to become similar following extended training leading to a more automatized (skilled) task performance which needs investigation in a future longitudinal ctDCS+VbaT therapy study. Also, computational neuroanatomy for motor control [64, 65] suggests specific functions of different parts of the brain where the cerebellum builds internal models that predict motor commands' sensory outcome and correct motor commands through internal feedback. Here, fMRI studies have shown decreased cerebellum activation with increased motor skill acquisition [66]. Therefore, ctDCS facilitating the cerebellar role is important in facilitating increased use of the paretic leg during biped tasks, including gait, where mean electric field strength at the cerebellar lobules was found to be positively related to the changes in the gait parameters of the affected leg [27]. Based on our prior work [27], we postulate that the VBaT paradigm [24] encouraging hemiplegic stroke survivors to learn an increased use of their paretic leg resulted in the ctDCS effects on the gait parameters of the affected leg, which needs further investigation in the future. In the current study, the contra-lesional (un-affected) SMC showed an increased activation based on the canonical score of O2Hb. In SMC, M1 and the premotor cortices are related to the implementation of the motor commands that are facilitated via cerebellar projections to M1 and premotor and other frontal regions [67]. After practice, the "motor" loop gets involved in developing "motor memory" [62] that consists of motor, premotor, somatosensory, supplementary motor areas, and anterior cerebellum that are involved in performance optimization (e.g., reduction in the reach errors). The premotor cortex has been implicated in the recombination and encoding of complex motor behaviors. So, fNIRS-EEG activation at SMC can be maximally targeted, as the "motor" loop gets involved, with tDCS electric field strength based on the reciprocity principle [12, 68]. Future neurophysiological studies need to combine fNIRS-EEG joint imaging of the ctDCS effects on the M1 activation with paired TMS to investigate motor skill learning

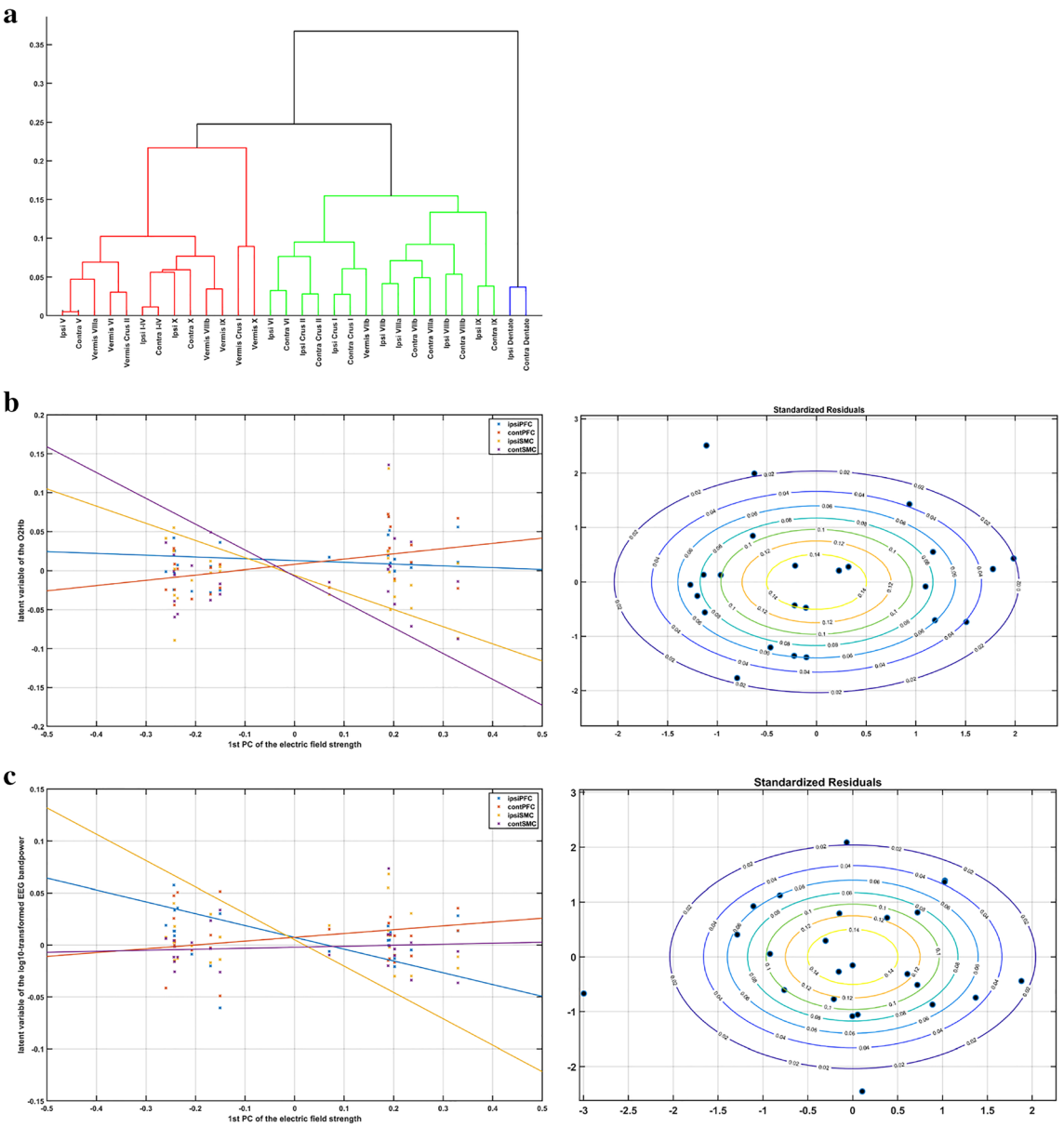


**Fig. 5** **a** Dendrogram plot of mean lobular electric field strength across subjects and ctDCS montages where the x-axis corresponds to the leaf nodes of the tree, and the y-axis corresponds to the linkage Euclidean distance between the three main clusters (in red, green, blue). **b** Left panel shows the general linear model fit with the PC1 of the mean lobular electric field strength as the predictor and the latent variables of the O2Hb as the response, while the right panel shows the standardized residuals of the regression model as the scatter plot with an overlay of a bivariate standard normal distribution. Here, for the regression model on the left panel, $ipsiPFC = 0.0128 + 0.0554 \times PC1 - 0.0783 \times PC2$; $contPFC = 0.0079 + 0.0758 \times PC1 - 0.0085 \times PC2$; $ipsiSMC = -0.0056 - 0.0199 \times PC1 - 0.2011 \times PC2$; $contSMC = -0.0068 + 0.0075 \times PC1 - 0.3394 \times PC2$. **c** Left panel shows the general linear model fit with the PC1 of the mean lobular electric field strength as the predictor and the latent variables of the log10-transformed EEG bandpower as the response, while the right panel shows the standardized residuals of the regression model as the scatter plot with an overlay of a bivariate standard normal distribution. Here, for the regression model on the left panel, $ipsiPFC = 0.0074 - 0.0228 \times PC1 - 0.0910 \times PC2$; $contPFC = 0.0075 - 0.0001 \times PC1 + 0.0370 \times PC2$; $ipsiSMC = 0.0051 + 0.0019 \times PC1 - 0.2558 \times PC2$; $contSMC = -0.0021 - 0.0023 \times PC1 + 0.0120 \times PC2$

where the CBI magnitude is postulated to decrease proportionally to the magnitude of motor skill learning [69].

Resting-state changes in the canonical scores of O2Hb can be related to the changes in the canonical scores of log10-transformed EEG bandpower based on a hemodynamic response function, as suggested by Keles et al. [70]. A significant effect of the state ($p$=0.0019) as well as the interaction between the ctDCS montage and the state ($p$=0.0153) were found on the changes in the canonical scores of log10-transformed EEG bandpower—see Fig. 3c, d. Here, log10-transformed EEG bandpower within 1–45 Hz covered five EEG frequency bands: δ (1–4 Hz), θ (4–7Hz), α (7–13 Hz),

β (13–30 Hz), and γ (30–45 Hz) where the α may generate β modulation of O2Hb-β coupling, as suggested by Keles et al. [70]. Figure 3d shows the interaction plots for the canonical scores of log10-transformed EEG bandpower where an increase across all ROIs can be found due to ctDCS. An increase in the canonical scores of log10-transformed EEG bandpower was higher at the ipsilesional PFC than contra-lesional PFC due to ctDCS of bilateral leg lobules VIIb-IX, while the opposite was found due to ctDCS of the dentate nuclei—see Fig. 3c. An increase in the canonical score for log10-transformed EEG bandpower may be related to decreased cortical excitability [25] due to contra-lesional anode (i.e., Δ*tDCS*) where ctDCS of bilateral leg lobules VIIb–IX primarily affected the inhibitory Purkinje cells while the ctDCS of dentate nuclei affected the excitatory dentato-thalamo-cortical pathway [62]. Here, cerebellar-brain inhibition [36] related ipsilesional effects of contra-lesional anode for ctDCS (i.e., Δ*tDCS*) were due to the inhibitory Purkinje cells. We found that ctDCS intervention (i.e., Δ*tDCS*) with bipolar Exx7 – Exx8 montage for bilateral leg lobules VIIb–IX led to a small decrease in the canonical scores for log10-transformed EEG bandpower at the contra-lesional ROIs that can be related to the "motor" loop—see Fig. 3a. However, during ctDCS (i.e., Δ*tDCS*) of dentate nuclei there was an increase in the canonical scores of log10-transformed EEG bandpower at the contra-lesional PFC (see Fig. 3 c and d) that can be related to the "cognitive" cortico-striatal loop [62]. Also, VBaT before ctDCS intervention (i.e., ΔpretDCS) as well as the VBaT after ctDCS intervention (i.e., ΔpostDCS) led to a decrease in the canonical scores of log10-transformed EEG bandpower, especially at the ipsilesional PFC—see Fig. 3d. Here, a decrease in the canonical score for log10-transformed EEG bandpower indicates increased cortical excitability [25] at both PFCs. These preliminary results indicated that fNIRS-EEG joint-imaging of the ctDCS effects on the cerebral activation could provide insights into the ctDCS effects on the motor skill learning [12, 15] during VBaT. Dutta et al. [65] highlighted the role of trial-by-trial error correction during such balance training where a decreased error or increased correct actions elicited a stronger alpha suppression (alpha event-related desynchronization), as shown by Pezzetta et al. too [71].

A dissociation in motor skill acquisition and retention processes has been postulated where ctDCS of the posterior cerebellum, including Crus I/II, can reduce movement errors during skill acquisition while M1 tDCS can facilitate increased retention of the new skill [72] after extensive practice. However, prior works in ctDCS [72] based on Celnik montage primarily affected the posterior cerebellum, related to the "cognitive" cortico-striatal loop [62] including the lobules Crus I/II, VIIb, VIII, and IX of the targeted cerebellar hemisphere, as elucidated by our CLOS study [21]. In the current study, we have showed the importance of lobule-specific electric field modeling in Fig. 2c where the bipolar PO9h – PO10h montage for dentate nuclei affected both the anterior and posterior lobes of the cerebellum (including Crus I–Crus II) while the bipolar Exx7 – Exx8 montage for bilateral leg lobules VIIb–IX primarily affected the posterior lobes of the cerebellum (excluding Crus I–Crus II). Furthermore, hierarchical cluster analysis of the mean lobular electric field strength across all subjects showed three separate clusters for the dentate nuclei and the cerebellar hemispheric lobules Crus I–Crus II along with the hemispheric lobules VIIb–IX for the two ctDCS montages—see Fig. 5a. Here, the dentate nuclei cluster was found to be well separated from the other two clusters, likely due to the location of the dentate nuclei centered within the concave shape of the cerebellar hemispheres. Due to the location of the dentate nuclei, conventional ctDCS montages, e.g., Celnik, Manto, and Extracephalic, can also strongly affect the dentate nucleus, so the functional effects of conventional ctDCS montages should be investigated based on the electric field effects on the dentate nucleus too [22]. Here, ctDCS of the dentate nuclei (i.e., ΔtDCS) may target the excitatory source of dense disynaptic projection to the striatum [73] where recent work also established functional territories [74]; specifically, a functional connection was shown to the medial prefrontal cortex. Also, ctDCS of the dentate nuclei is postulated to be faciliatory (excitatory to the cortico-striatal circuit) for operant conditioning VBaT [24] with reward feedback acting via basal ganglia [73] that can facilitate motor learning [75]. In contrast, ctDCS targeting the bilateral leg lobules VIIb-IX via inhibitory Purkinje cells may facilitate distinct error-based learning [65, 73] that is driven by M1—"motor" loop. We postulate that such trial-by-trial error correction during a functional reach standing balance task [23] can be facilitated with ctDCS, where the cerebral responses can be recorded with fNIRS-EEG join-imaging for monitoring ctDCS effects on the trial-by-trial error correction. Based on prior works, we further postulate that performance during the initial stages of the VR balance learning task [23] is mainly based on trial-by-trial error exploration involving the ventromedial prefrontal cortex, ventral striatum, and posterior cerebellum [73]. As the learning progresses, then the "cognitive" cortico-striatal loop gets involved that consists of the dorsolateral prefrontal cortex, dorsomedial striatum, and lateral posterior cerebellum [62] when working memory access is crucial [73]. Finally, after extensive practice, the "motor" loop gets involved in developing "motor memory" that consists of motor, premotor, somatosensory, supplementary motor areas, and anterior cerebellum that are engaged in performance optimization [62]. Therefore, ctDCS of the anterior cerebellum may facilitate the development of "motor memory" [62] after extensive practice.

Our preliminary fNIRS-EEG results (see Fig. 3) showed differences in the cerebral activation, especially in the canonical scores of O2Hb, due to VBaT as well as its interaction with ctDCS of the combined anterior and posterior lobes of

cerebellum versus ctDCS of the posterior lobes of the cerebellum. So, fNIRS-EEG-based imaging of cerebral responses may enable dynamic tDCS targeting the moving cerebral sources during ctDCS facilitated motor learning using current steering under the reciprocity principle [12, 68]. This can allow staggered delivery of ctDCS for motor skill learning based on fNIRS-EEG joint-imaging, especially in stroke survivors with heterogeneous deficits based on the postulated shift in the peak activation from PFC to SMC in the responders. Moreover, ctDCS targeting specific regions of the cerebellum required optimization of cerebellar lobule-specific electric field distribution made possible by our Cerebellar Lobules Optimal Stimulation pipeline [21]. In the current study, the CLOS pipeline provided age-appropriate optimization of the ctDCS electrode montage [29] for bilateral ctDCS of the dentate nucleus and lower-limb representations (lobules VII-IX) [22], which was proposed to facilitate standing balance learning in chronic stroke survivors. The cerebrum activity was investigated in this methodological study based on our prior works on simultaneous fNIRS-EEG imaging of tDCS-evoked neurovascular responses [8, 10, 35]. Here, neurovascular coupling represents interactions within the "neurovascular unit" (NVU), consisting of neuronal, glial, and vascular cells. Although focal hemodynamic tDCS effects [16, 26] in the targeted brain areas can be due to the electric field directly affecting the neurons, astrocytes, as well as the vascular cells within the NVU [35]; yet, any remote hemodynamic effects in the cerebrum areas unaffected directly by the ctDCS electric field can be postulated to be driven by brain connectivity [47, 76]. Briefly, neuronal activation driven by brain connectivity [77] facilitated with remote tDCS [78] can be accompanied by increased cerebral blood flow and increased cerebral metabolic rate for oxygen, leading to functional hyperemia and energy supply. This methodological study performed fNIRS-EEG joint-imaging covering the prefrontal cortex, the primary motor cortex, and the supplementary motor area to investigate the ctDCS effects. Offline resting-state ctDCS was performed to identify the priming effects of ctDCS on the cerebral regions, which can then modulate the brain activation during standing balance learning VBaT task. Our simultaneous fNIRS-EEG combined EEG and fNIRS benefits by applying multimodal subspace signal processing to identify latent coupling variables using canonical correlation analysis [78] while avoiding the logistical challenges associated with fMRI-EEG in a rehabilitation setting. Here, CCA aimed to maximize the correlation between EEG band power and fNIRS measure tHb across relevant frequency bands to identify latent variables that may be less susceptible to systemic artefacts in fNIRS data. Specifically, we aimed for non-invasive and simultaneous assessment of the neuronal activity and hemodynamic responses to priming by resting-state bilateral ctDCS. In contrast to our prior results [8] that found high-definition M1 tDCS effects on the coupling between the log10-transformed EEG bandpower within 1–45 Hz and the O2HB signals in the low-frequency band (≤0.1 Hz) in the neurovascular tissue underlying HD-tDCS 4 × 1 electrodes, we did not find ctDCS electric field effects in the current study. Moreover, canonical correlations were not significant between the log10-transformed EEG bandpower within 1–45 Hz and the tHb signals within the neurovascular coupling band (0.01–0.07Hz) [59]. This showed that ctDCS did not have a significant effect on the cerebral neurovascular coupling that can be related to postulated neural efficiency or increased neuronal performance that negatively modulated increases in hemodynamic activity [17, 18].

This study's limitations include "one-size-fits-all" ctDCS electrode montages; however, we performed computational modeling of the electric field using age-appropriate human brain MRI templates that were used as predictors in the multivariate GLM. We used subject-matched age-groups for computational modeling to estimate electric field stimulation for the patients who had no lesion in the cerebellum (clinical notes based on CT scan at the stroke onset). In this feasibility study on chronic stroke subjects in low-resource settings, we did not have IRB approved access to the CT scans so differences in the individual cerebellar anatomy and residual connectivity can play an essential role in the efficacy of the ctDCS [79], which may have resulted in the inter-subject variability. Indeed, two chronic post-stroke subjects with upper-limb IMA had a poor fit to the regression model, shown by the standardized residuals ($p<0.04$) in Fig. 5 b and c, who also performed poorly in terms of VBaT target reaching success rate [22]. Therefore, multivariate GLM presented in this study needs further investigation in a larger cohort to identify post-stroke non-responders to ctDCS (i.e., based on ΔtDCS). Here, VBaT performance in IMA may be affected by subcortical dysfunction in the basal ganglia motor circuit [80]. Therefore, a large clinical study using VBaT and fNIRS-EEG joint-imaging is necessary to elucidate the inconsistency in lobule-specific ctDCS effects based on individual residual function [36, 81]. For example, ctDCS has shown promise in improving standing balance performance in small studies with fifteen patients with chronic stroke (>6 months post-stroke) [13] where exploration of optimal timing, dose, and the relation between qualitative parameters, and clinical improvements are necessary. This is important since a recent study [82] showed that multiple sessions (three sessions of 20 min per week for 2 weeks) of simultaneous postural training with bilateral anodal ctDCS (not postural training or bilateral anodal ctDCS alone) was necessary to deliver therapeutic effects in older adults with high fall risk. Here, a GLM analysis between the ctDCS electric field and the latent variables for fNIRS-EEG coupling response may elucidate post-stroke functional brain connectivity that may correlate with white matter structural integrity in the corresponding cerebello-thalamo-cortical white matter tract [76]. Future clinical studies with a bigger

sample size are required for unraveling the systematic effects of the optimized ctDCS for different cerebellar regions using the multivariate GLM approach presented in this study. In the current study, response variables in the multivariate GLM consisted of recordings from a low-density (8-channel) fNIRS-EEG system that provided limited PFC and SMC coverage (only four ROIs studied). Also, due to a limited number of available fNIRS channels, we could not allocate short-distance probes to reduce global interference of scalp-hemodynamics in our GLM to reduce fNIRS susceptibility to false positives [83]. Nevertheless, the canonical scores for fNIRS O2Hb and HHb signal in the latent space are postulated to be less sensitive to the systemic artifacts that need to be validated in a future study short-channel regression [84]. We found good scalp coupling of the fNIRS optodes at the PFC based on the PHOEBE approach that showed decreased activation in the contra-lesional PFC with increased VBaT training at the first exposure of novice stroke survivors. Also, future improvement in the fNIRS sensitivity using silicon photomultipliers [85] can improve the brain imaging of the hair areas including SMC that may reduce variability in the data. In the current study, low-density fNIRS-EEG allowed sensor placement on the head in a short amount of time that is important for clinical translation in a low-resource point-of-care setting [86] used for our current feasibility study. Our ongoing work is focused on the improvement of the fNIRS-EEG signal fidelity for monitoring the dynamical changes in brain activation associated with ctDCS facilitated VBaT balance training in stroke survivors.

## Conclusion

The feasibility of portable fNIRS-EEG neuroimaging of the cerebral cortex response to focal ctDCS was shown in this methodological study vis-à-vis lobular electric field strength using two-electrode montages. We demonstrated the feasibility of principal component regression to relate the mean lobular electric field strength as the predictor to the latent variable of the O2Hb as the response. Here, chronic post-stroke subjects with upper-limb IMA who performed poorly in the VBaT tasks also had a poor fit to the regression model. This showed the importance of subject-specific residual architecture for cerebellar interconnections with the cerebral cortex, including the prefrontal cortex and the sensorimotor cortex, which affected the ctDCS response in terms of cerebral functional activation.

**Supplementary Information** The online version contains supplementary material available at https://doi.org/10.1007/s12311-021-01249-4.

**Acknowledgements** The authors would like to acknowledge the technical support from Brandon Ruszala for the development of the CLOS pipeline and the clinical support from Surbhi Kaura for the MRIs and the stroke study at the All India Institute of Medical Sciences, New Delhi, India. Deepesh Kumar conducted initial technology development and experimental validation of the VBaT platform during his doctoral research at the Indian Institute of Technology Gandhinagar, India.

**Author Contribution** Neuroimaging in conjunction with non-invasive brain stimulation study conceptualization and design, A.D. (Anirban Dutta); Virtual reality-based balance training conceptualization and design, U.L. (Uttama Lahiri); Methodology, Z.R. (Zeynab Rezaee), D.S. (Dhaval Solanki), S.R. (Shashi Ranjan), A.D., and U.L.; Software development and application, Z.R., D.S., M.B. (Mahasweta Bhattacharya); Investigation, Z.R., D.S., and S.R.; Resources, A.D. (Anirban Dutta), U.L., and M.V.P.S. (MV Padma Srivastava); Data curation, Z.R., D.S., and S.R.; Writing—original draft preparation, Z.R., D.S., A.D., and U.L.; Writing—review and editing, A.D., U.L., and M.V.P.S.; Supervision, A.D., and U.L.; Project administration, A.D., U.L., and M.V.P.S; Funding acquisition, A.D., U.L., and M.V.P.S. All authors have read and agreed to the published version of the manuscript.

**Funding** Authors acknowledge the initial funding (2014−2017) by the Department of Science and Technology (DST), India and Institut National de Recherche en Informatique et en Automatique (Inria), France—https://team.inria.fr/nphys4nrehab/. This research is currently funded by the Indian Ministry of Human Resource Development (MHRD)'s Scheme for Promotion of Academic and Research Collaboration (SPARC), grant number 2018−2019/P721/SL, and Indian Department of Health Research, Project Code No. N1761.

## Declarations

**Conflict of Interest** The authors declare no competing interests.

## References

1. van Dun K, Manto M. Non-invasive cerebellar stimulation: moving towards clinical applications for cerebellar and extra-cerebellar disorders. Cerebellum. 2018;17:259–63.
2. Koch G, Bonnì S, Casula EP, Iosa M, Paolucci S, Pellicciari MC, et al. Effect of cerebellar stimulation on gait and balance recovery in patients with hemiparetic stroke: a randomized clinical trial. JAMA Neurol. 2019;76:170–8.
3. Grimaldi G, Argyropoulos GP, Boehringer A, Celnik P, Edwards MJ, Ferrucci R, et al. Non-invasive cerebellar stimulation–a consensus paper. Cerebellum. 2014;13:121–38.
4. Dyke K, Kim S, Jackson GM, Jackson SR. Intra-subject consistency and reliability of response following 2 mA transcranial direct current stimulation. Brain Stimul. 2016;9:819–25.
5. Van de Winckel A, Carey JR, Bisson TA, Hauschildt EC, Streib CD, Durfee WK. Home-based transcranial direct current stimulation plus tracking training therapy in people with stroke: an open-label feasibility study. J NeuroEng Rehabil. 2018;15:83.
6. Carvalho F, Brietzke AP, Gasparin A, Dos Santos FP, Vercelino R, Ballester RF, et al. Home-based transcranial direct current stimulation device development: an updated protocol used at home in healthy subjects and fibromyalgia patients. J Vis Exp. 2018;(137):57614. https://doi.org/10.3791/57614
7. Brunoni AR, Nitsche MA, Bolognini N, Bikson M, Wagner T, Merabet L, et al. Clinical research with transcranial direct current stimulation (tDCS): challenges and future directions. Brain Stimul. 2012;5:175–95.

8. Dutta A, Jacob A, Chowdhury SR, Das A, Nitsche MA. EEG-NIRS based assessment of neurovascular coupling during anodal transcranial direct current stimulation–a stroke case series. J Med Syst. 2015;39:205.
9. Girouard H, Iadecola C. Neurovascular coupling in the normal brain and in hypertension, stroke, and Alzheimer disease. J Appl Physiol. 2006;100:328–35.
10. Koo B, Lee H-G, Nam Y, Kang H, Koh CS, Shin H-C, et al. A hybrid NIRS-EEG system for self-paced brain computer interface with online motor imagery. J Neurosci Methods. 2015;244:26–32.
11. Quaresima V, Ferrari M. Functional Near-Infrared Spectroscopy (fNIRS) for assessing cerebral cortex function during human behavior in natural/social situations: a concise review. Organ Res Methods. 2019;22:46–68.
12. Guhathakurta D, Dutta A. Computational pipeline for NIRS-EEG joint imaging of tDCS-evoked cerebral responses—an application in ischemic stroke. Front Neurosci [Internet]. 2016 [cited 2018 Jun 16];10. Available from: https://www.frontiersin.org/articles/10.3389/fnins.2016.00261/full.
13. Zandvliet SB, Meskers CGM, Kwakkel G, van Wegen EEH. Short-term effects of cerebellar tDCS on standing balance performance in patients with chronic stroke and healthy age-matched elderly. Cerebellum. 2018;17:575–89.
14. Ballard HK, Goen JRM, Maldonado T, Bernard JA. Effects of cerebellar transcranial direct current stimulation on the cognitive stage of sequence learning. J Neurophysiol. 2019;122:490–9.
15. Nemani A, Yücel MA, Kruger U, Gee DW, Cooper C, Schwaitzberg SD, et al. Assessing bimanual motor skills with optical neuroimaging. Sci Adv. 2018;4:eaat3807.
16. Sood M, Besson P, Muthalib M, Jindal U, Perrey S, Dutta A, et al. NIRS-EEG joint imaging during transcranial direct current stimulation: online parameter estimation with an autoregressive model. J Neurosci Methods. 2016;274:71–80.
17. Hunter MA, Lieberman G, Coffman BA, Trumbo MC, Armenta ML, Robinson CSH, et al. Mindfulness-based training with transcranial direct current stimulation modulates neuronal resource allocation in working memory: a randomized pilot study with a non-equivalent control group. Heliyon. 2018;4:e00685.
18. McKendrick R, Parasuraman R, Ayaz H. Wearable functional near infrared spectroscopy (fNIRS) and transcranial direct current stimulation (tDCS): expanding vistas for neurocognitive augmentation. Front Syst Neurosci [Internet]. Frontiers; 2015 [cited 2020 Sep 9];9. Available from: https://www.frontiersin.org/articles/10.3389/fnsys.2015.00027/full.
19. Batsikadze G, Rezaee Z, Chang D-I, Gerwig M, Herlitze S, Dutta A, et al. Effects of cerebellar transcranial direct current stimulation on cerebellar-brain inhibition in humans: a systematic evaluation. Brain Stimulation: Basic, Translational, and Clinical Research in Neuromodulation [Internet]. 2019 [cited 2019 Jun 15];0. Available from: https://www.brainstimjrnl.com/article/S1935-861X(19)30201-3/abstract.
20. Fernandez L, Major BP, Teo W-P, Byrne LK, Enticott PG. Assessing cerebellar brain inhibition (CBI) via transcranial magnetic stimulation (TMS): A systematic review. Neurosci Biobehav Rev. 2018;86:176–206.
21. Rezaee Z, Dutta A. Cerebellar Lobules Optimal Stimulation (CLOS): A computational pipeline to optimize cerebellar lobule-specific electric field distribution. Front Neurosci [Internet]. 2019 [cited 2019 Jun 15];13. Available from: https://www.frontiersin.org/articles/10.3389/fnins.2019.00266/full#B5.
22. Rezaee Z, Kaura S, Solanki D, Dash A, Srivastava MVP, Lahiri U, et al. Deep cerebellar transcranial direct current stimulation of the dentate nucleus to facilitate standing balance in chronic stroke survivors—a pilot study. Brain Sci. 2020;10:94.
23. Verma S, Kumar D, Kumawat A, Dutta A, Lahiri U. A Low-Cost Adaptive Balance Training Platform for Stroke Patients: A Usability Study. IEEE Trans Neural Syst Rehabil Eng. 2017;25:935–44.
24. Kumar D, Sinha N, Dutta A, Lahiri U. Virtual reality-based balance training system augmented with operant conditioning paradigm. Biomed Eng Online. 2019;18:90.
25. Jindal U, Sood M, Chowdhury SR, Das A, Kondziella D, Dutta A. Corticospinal excitability changes to anodal tDCS elucidated with NIRS-EEG joint-imaging: an ischemic stroke study. Conf Proc IEEE Eng Med Biol Soc. 2015;2015:3399–402.
26. Muthalib M, Besson P, Rothwell J, Perrey S. Focal hemodynamic responses in the stimulated hemisphere during high-definition transcranial direct current stimulation. Neuromodulation. 2018;21:348–54.
27. Solanki D, Rezaee Z, Dutta A, Lahiri U. Investigating the feasibility of cerebellar transcranial direct current stimulation to facilitate post-stroke overground gait performance in chronic stroke: a partial least-squares regression approach. J NeuroEng Rehabil. 2021;18:18.
28. Guell X, Schmahmann JD, Gabrieli JD, Ghosh SS. Functional gradients of the cerebellum. Bostan A, Ivry RB, editors. eLife. 2018;7:e36652.
29. Rezaee Z, Dutta A. Lobule-specific dosage considerations for cerebellar transcranial direct current stimulation during healthy aging: a computational modeling study using age-specific magnetic resonance imaging templates. Neuromodulation. 2020;23:341–65.
30. Abadi ZRH, Dutta A. Optimizing cerebellar transcranial direct current stimulation for visuomotor learning - anterior versus posterior lobe of cerebellum. 2017 8th International IEEE/EMBS Conference on Neural Engineering (NER). 2017. p. 428–31.
31. Buckner RL, Krienen FM, Castellanos A, Diaz JC, Yeo BTT. The organization of the human cerebellum estimated by intrinsic functional connectivity. J Neurophysiol. 2011;106:2322–45.
32. Stoodley CJ, Valera EM, Schmahmann JD. Functional topography of the cerebellum for motor and cognitive tasks: an fMRI study. Neuroimage. 2012;59:1560–70.
33. Guell X, Schmahmann J. Cerebellar functional anatomy: a didactic summary based on human fMRI evidence. Cerebellum. 2020;19:1–5.
34. Wittenberg E, Thompson J, Nam CS, Franz JR. Neuroimaging of human balance control: a systematic review. Front Hum Neurosci [Internet]. 2017 [cited 2019 Jun 25];11. Available from: https://www.ncbi.nlm.nih.gov/pmc/articles/PMC5385364/.
35. Dutta A. Bidirectional interactions between neuronal and hemodynamic responses to transcranial direct current stimulation (tDCS): challenges for brain-state dependent tDCS. Front Syst Neurosci. 2015;9:107.
36. Grimaldi G, Argyropoulos GP, Bastian A, Cortes M, Davis NJ, Edwards DJ, et al. Cerebellar transcranial direct current stimulation (ctDCS). Neuroscientist. 2016;22:83–97.
37. Berg KO, Wood-Dauphinee SL, Williams JI, Maki B. Measuring balance in the elderly: validation of an instrument. Can J Public Health. 1992;83(Suppl 2):S7–11.
38. Fillmore PT, Phillips-Meek MC, Richards JE. Age-specific MRI brain and head templates for healthy adults from 20 through 89 years of age. Front Aging Neurosci [Internet]. 2015 [cited 2020 Sep 9];7. Available from: https://www.ncbi.nlm.nih.gov/pmc/articles/PMC4389545/.
39. Huang Y, Datta A, Bikson M, Parra LC. ROAST: an open-source, fully-automated, realistic volumetric-approach-based simulator for TES. Conf Proc IEEE Eng Med Biol Soc. 2018;2018:3072–5.
40. SPM - Statistical Parametric Mapping [Internet]. [cited 2018 Jun 16]. Available from: http://www.fil.ion.ucl.ac.uk/spm/.
41. Fang Q, Boas DA. Tetrahedral mesh generation from volumetric binary and grayscale images. 2009 IEEE International Symposium on Biomedical Imaging: From Nano to Macro. 2009. p. 1142–5.

42. Dular P, Geuzaine C, Henrotte F, Legros W. A general environment for the treatment of discrete problems and its application to the finite element method. IEEE Trans Magn. 1998;34:3395–8.
43. Windhoff M, Opitz A, Thielscher A. Electric field calculations in brain stimulation based on finite elements: an optimized processing pipeline for the generation and usage of accurate individual head models. Hum Brain Mapp. 2013;34:923–35.
44. Diedrichsen J. A spatially unbiased atlas template of the human cerebellum. Neuroimage. 2006;33:127–38.
45. Geng S, Liu X, Biswal BB, Niu H. Effect of resting-state fNIRS scanning duration on functional brain connectivity and graph theory metrics of brain network. Front Neurosci [Internet]. Frontiers; 2017 [cited 2021 Jan 30];11. Available from: https://www.frontiersin.org/articles/10.3389/fnins.2017.00392/full.
46. Othman MH, Bhattacharya M, Møller K, Kjeldsen S, Grand J, Kjaergaard J, et al. Resting-state NIRS-EEG in unresponsive patients with acute brain injury: a proof-of-concept study. Neurocrit Care. 2020. https://doi.org/10.1007/s12028-020-00971-x.
47. Krienen FM, Buckner RL. Segregated fronto-cerebellar circuits revealed by intrinsic functional connectivity. Cereb Cortex. 2009;19:2485–97.
48. Angulo-Sherman IN, Rodríguez-Ugarte M, Sciacca N, Iáñez E, Azorín JM. Effect of tDCS stimulation of motor cortex and cerebellum on EEG classification of motor imagery and sensorimotor band power. J NeuroEng Rehabil. 2017;14:31.
49. Aasted CM, Yücel MA, Cooper RJ, Dubb J, Tsuzuki D, Becerra L, et al. Anatomical guidance for functional near-infrared spectroscopy: AtlasViewer tutorial. Neurophotonics [Internet]. 2015 [cited 2020 Apr 18];2. Available from: https://www.ncbi.nlm.nih.gov/pmc/articles/PMC4478785/.
50. Pinti P, Merla A, Aichelburg C, Lind F, Power S, Swingler E, et al. A novel GLM-based method for the Automatic IDentification of functional Events (AIDE) in fNIRS data recorded in naturalistic environments. Neuroimage. 2017;155:291–304.
51. Chang C-Y, Hsu S-H, Pion-Tonachini L, Jung T-P. Evaluation of artifact subspace reconstruction for automatic artifact components removal in multi-channel EEG recordings. IEEE Trans Biomed Eng. 2020;67:1114–21.
52. Hsu S-H, Pion-Tonachini L, Palmer J, Miyakoshi M, Makeig S, Jung T-P. Modeling brain dynamic state changes with adaptive mixture independent component analysis. Neuroimage. 2018;183:47–61.
53. Pion-Tonachini L, Kreutz-Delgado K, Makeig S. The ICLabel dataset of electroencephalographic (EEG) independent component (IC) features. Data Brief. 2019;25:104101.
54. Chaumon M, Bishop DVM, Busch NA. A practical guide to the selection of independent components of the electroencephalogram for artifact correction. J Neurosci Methods. 2015;250:47–63.
55. Tachtsidis I, Scholkmann F. False positives and false negatives in functional near-infrared spectroscopy: issues, challenges, and the way forward. Neurophotonics [Internet]. 2016 [cited 2019 Sep 29];3. Available from: https://www.ncbi.nlm.nih.gov/pmc/articles/PMC4791590/.
56. Pollonini L, Bortfeld H, Oghalai JS. PHOEBE: a method for real time mapping of optodes-scalp coupling in functional near-infrared spectroscopy. Biomed Opt Express. 2016;7:5104–19.
57. von Lühmann A, Li X, Müller K-R, Boas DA, Yücel MA. Improved physiological noise regression in fNIRS: a multimodal extension of the general linear model using temporally embedded canonical correlation analysis. NeuroImage. 2020;208:116472.
58. Zhang Y, Brooks DH, Franceschini MA, Boas DA. Eigenvector-based spatial filtering for reduction of physiological interference in diffuse optical imaging. J Biomed Opt. 2005;10:11014.
59. Tan Q, Zhang M, Wang Y, Zhang M, Wang Y, Xin Q, et al. Frequency-specific functional connectivity revealed by wavelet-based coherence analysis in elderly subjects with cerebral infarction using NIRS method. Med Phys. 2015;42:5391–403.
60. Alkire MT. Quantitative EEG correlations with brain glucose metabolic rate during anesthesia in volunteers. Anesthesiology. 1998;89:323–33.
61. Zadikoff C, Lang AE. Apraxia in movement disorders. Brain. 2005;128:1480–97.
62. Marinelli L, Quartarone A, Hallett M, Frazzitta G, Ghilardi MF. The many facets of motor learning and their relevance for Parkinson's disease. Clin Neurophysiol. 2017;128:1127–41.
63. Vandaele Y, Mahajan NR, Ottenheimer DJ, Richard JM, Mysore SP, Janak PH. Distinct recruitment of dorsomedial and dorsolateral striatum erodes with extended training. Wassum KM, Uchida N, Uchida N, Robbe D, editors. eLife. 2019;8:e49536.
64. Shadmehr R, Smith MA, Krakauer JW. Error correction, sensory prediction, and adaptation in motor control. Annu Rev Neurosci. 2010;33:89–108.
65. Dutta A, Lahiri U, Das A, Nitsche MA, Guiraud D. Post-stroke balance rehabilitation under multi-level electrotherapy: a conceptual review. Front Neurosci [Internet]. 2014 [cited 2018 Jun 20];8. Available from: https://www.ncbi.nlm.nih.gov/pmc/articles/PMC4266025/.
66. Friston KJ, Frith CD, Passingham RE, Liddle PF, Frackowiak RSJ. Motor practice and neurophysiological adaptation in the cerebellum: a positron tomography study. Proc R Soc Lond Ser B Biol Sci R Soc. 1992;248:223–8.
67. Bostan AC, Dum RP, Strick PL. Cerebellar networks with the cerebral cortex and basal ganglia. Trends Cogn Sci (Regul Ed). 2013;17:241–54.
68. Dutta A, Dutta A. Using electromagnetic reciprocity and magnetic resonance current density imaging to fit multi-electrode montage for non-invasive brain stimulation. 2013 6th International IEEE/EMBS Conference on Neural Engineering (NER). 2013. p. 447–51.
69. Celnik P. Understanding and modulating motor learning with cerebellar stimulation. Cerebellum. 2015;14:171–4.
70. Keles HO, Barbour RL, Omurtag A. Hemodynamic correlates of spontaneous neural activity measured by human whole-head resting state EEG+fNIRS. Neuroimage. 2016;138:76–87.
71. Pezzetta R, Nicolardi V, Tidoni E, Aglioti SM. Error, rather than its probability, elicits specific electrocortical signatures: a combined EEG-immersive virtual reality study of action observation. J Neurophysiol. 2018;120:1107–18.
72. Galea JM, Vazquez A, Pasricha N, Orban de Xivry J-J, Celnik P. Dissociating the roles of the cerebellum and motor cortex during adaptive learning: the motor cortex retains what the cerebellum learns. Cereb Cortex. 2011;21:1761–70.
73. Bostan AC, Strick PL. The basal ganglia and the cerebellum: nodes in an integrated network. Nat Rev Neurosci. 2018;19:338–50.
74. Guell X, D'Mello AM, Hubbard NA, Romeo RR, Gabrieli JDE, Whitfield-Gabrieli S, et al. Functional territories of human dentate nucleus. Cereb Cortex [Internet]. [cited 2020 Mar 7]; Available from: https://academic.oup.com/cercor/advance-article/doi/10.1093/cercor/bhz247/5614447.
75. Spampinato DA, Satar Z, Rothwell JC. Combining reward and M1 transcranial direct current stimulation enhances the retention of newly learnt sensorimotor mappings. Brain Stimul. 2019;12:1205–12.
76. Bernard JA, Orr JM, Mittal VA. Differential motor and prefrontal cerebello-cortical network development: evidence from multimodal neuroimaging. NeuroImage. 2016;124:591–601.
77. Di Lazzaro V, Rothwell JC. Corticospinal activity evoked and modulated by non-invasive stimulation of the intact human motor cortex. J Physiol. 2014;592:4115–28.
78. Polanía R, Nitsche MA, Ruff CC. Studying and modifying brain function with non-invasive brain stimulation. Nat Neurosci. 2018;21:174–87.

79. Oldrati V, Schutter DJLG. Targeting the human cerebellum with transcranial direct current stimulation to modulate behavior: a meta-analysis. Cerebellum. 2018;17:228–36.
80. Hanna-Pladdy B, Heilman KM, Foundas AL. Cortical and subcortical contributions to ideomotor apraxia: analysis of task demands and error types. Brain. 2001;124:2513–27.
81. Jalali R, Miall RC, Galea JM. No consistent effect of cerebellar transcranial direct current stimulation on visuomotor adaptation. J Neurophysiol. 2017;118:655–65.
82. Yosephi MH, Ehsani F, Zoghi M, Jaberzadeh S. Multi-session anodal tDCS enhances the effects of postural training on balance and postural stability in older adults with high fall risk: primary motor cortex versus cerebellar stimulation. Brain Stimul. 2018;11:1239–50.
83. Sato T, Nambu I, Takeda K, Aihara T, Yamashita O, Isogaya Y, et al. Reduction of global interference of scalp-hemodynamics in functional near-infrared spectroscopy using short distance probes. NeuroImage. 2016;141:120–32.
84. Gagnon L, Cooper RJ, Yücel MA, Perdue KL, Greve DN, Boas DA. Short separation channel location impacts the performance of short channel regression in NIRS. Neuroimage. 2012;59:2518–28.
85. Pagano R, Libertino S, Sanfilippo D, Fallica G, Lombardo S. Improvement of sensitivity in continuous wave near infra-red spectroscopy systems by using silicon photomultipliers. Biomed Opt Express. 2016;7:1183–92.
86. Dutta A, Nitsche WP and MA. Translational methods for non-invasive electrical stimulation to facilitate gait rehabilitation following stroke - the future directions [Internet]. Neuroscience and Biomedical Engineering (Discontinued). 2013 [cited 2020 Sep 9]. p. 22–33. Available from: https://www.eurekaselect.com/109867/article.